Hallmarks of uterine receptivity predate placental mammals

Silvia Basanta[o*1], Daniel J. Stadtmauer[o*1,2], Jamie D. Maziarz[2,3], Caitlin E. McDonough-Goldstein[1,4], Alison G. Cole[5], Gülay Dagdas[1], Günter P. Wagner[o1,2,6], Mihaela Pavličev[o1,7]

1. Department of Evolutionary Biology, University of Vienna, Vienna, Austria
2. Department of Ecology & Evolutionary Biology, Yale University, New Haven, CT, USA
3. Department of Molecular, Cellular, and Developmental Biology, Yale University, New Haven, CT, USA
4. Department of Integrative Biology, University of Wisconsin-Madison, WI, USA
5. Department of Neuroscience and Developmental Biology, University of Vienna, Vienna, Austria
6. Department of Animal Science, Texas A&M University, College Station, TX, USA
7. Complexity Science Hub Vienna, Vienna, Austria

ORCID: Silvia Basanta: 0000-0002-3161-959X; Daniel Stadtmauer: 0000-0001-6249-5924; Günter Wagner: 0000-0002-3097-002X; Mihaela Pavlicev: 0000-0001-8439-9351; Alison G. Cole: 0000-0002-7515-7489

[o]Corresponding authors:

silvia.basanta@univie.ac.at

daniel.stadtmauer@yale.edu

gunter.wagner@yale.edu

mihaela.pavlicev@univie.ac.at

*These authors contributed equally

Abstract

Embryo implantation requires tightly coordinated signaling between the blastocyst and the endometrium, and is crucial for the establishment of a uteroplacental unit that persists until term in eutherian mammals. In contrast, marsupials, with a unique life cycle and short gestation, make only brief fetal-maternal contact and lack implantation. To better understand the evolutionary link between eutherian implantation and its ancestral equivalent in marsupials, we compare single-cell transcriptomes from the receptive and non-receptive endometrium of the mouse and guinea pig with that of the opossum, a marsupial. We identify substantial differences between rodent peri-implantation endometrium and opossum placental attachment, including differences in the diversity and abundance of stromal and epithelial cells which parallel the difference between histotrophic and hemotrophic provisioning strategies. We also identify a window of conserved epithelial gene expression between the opossum shelled blastocyst stage and rodent peri-implantation, including *IHH* and *LIF*. We find strong conservation of blastocyst proteases, steroid synthetases, Wnt and BMP signals between eutherians and the opossum despite its lack of implantation. Finally, we show that the signaling repertoire of the maternal uterine epithelium during implantation displays substantial overlap with that of the post-implantation placental trophoblast, suggesting that the fetal trophoblast can compensate for the loss of endometrial epithelium in eutherian invasive placentation. Together, our results suggest that eutherian implantation primarily involved the re-wiring of maternal signaling networks, some of which were already present in the therian ancestor, and points towards an essential role of maternal innovations in the evolution of invasive placentation.

Introduction

Embryo implantation constitutes the first direct fetal-maternal encounter. It involves the blastocyst's apposition, adhesion, and - in species with invasive placentation - invasion of the blastocyst into the endometrium (Schlafke & Enders, 1975). In contrast to other forms of fetal-maternal contact, implantation involves breaching to some degree the maternal luminal epithelium by the embryo. Adhesion of the trophectoderm to the luminal epithelium requires modifications in cellular polarity on both sides (Denker, 1993). Disrupting endometrial integrity during the invasion by a semi-allogeneic embryo, on the other hand, requires taming of the inflammatory reaction (Griffith et al., 2017), a wound healing response (Nancy et al., 2018; Osokine et al., 2022), as well as avoiding immune rejection of the embryo (Medawar, 1953). Maternal innovations to overcome these challenges were necessary for implantation to evolve (Stadtmauer & Wagner, 2020a; Wagner, forthcoming).

Reconstructing the evolutionary origin of the sequence of developmental events involved in embryo implantation is difficult because of the lack of intermediate phenotypes. Invasive implantation likely evolved in the stem lineage of eutherian mammals (Wildman et al., 2006), coincident with invasive placentation and with the origin of the decidual reaction and the decidual stromal cell type (Mess & Carter, 2006). The type of epithelial penetration, the degree of invasion, and the orientation of the blastocyst upon attachment vary significantly even across closely related eutherian species (Siriwardena & Boroviak, 2022).

Implantation success depends on both the competency of the blastocyst and the receptivity of the endometrium. Success is determined by blastocyst chromosomal integrity and by maternal viability checkpoints (reviewed in Muter et al., 2023). It also depends upon endometrial remodeling of the epithelium and stroma, immune cell recruitment, vascular growth, and development of secretory endometrial glands. While several of these processes occur as part of the endometrial cycle

regardless of fertilization, others are triggered and enhanced by the presence of the embryo. Endometrial remodeling unique to pregnant cycles is known as “endometrial recognition of pregnancy” (Renfree, 2000), as opposed to “endocrine recognition of pregnancy”, which refers to serum levels of progesterone and estradiol differing significantly between pregnant and estrous cycles (Harder and Fleming, 1981). The latter is a derived characteristic of eutherian pregnancy. The blastocyst stage displays substantial morphological and developmental differences across mammals (Frankenberg et al., 2016), but also striking transcriptomic similarities at the cell type level of the embryo (Malkowska et al., 2022). However, the degree of evolutionary conservation in signaling between the blastocyst and the mother has remained unknown.

Much of what we know about eutherian implantation comes from mouse models, including genetically modified knockout mouse lines and their reproductive phenotypes (Dey et al., 2004, Wang & Dey, 2006). Aspects of implantation are variable across eutherians, and relying on single species thus confounds the species-specific characteristics with those of the larger group. In order to better represent rodents, we can look to a representative of the most basally branching rodent group, the guinea pig, with a long estrus cycle of around 16 days and an interstitial implantation phenotype resembling the human and differing from eccentric implantation of the mouse (Lee & DeMayo, 2004; Carter, 2007). The two species differ in the hormonal priming of the endometrium, with mouse pregnancy requiring a peri-implantation estrogen peak but not the guinea pig (Deanesly, 1960).

In contrast to rodents and other eutherian mammals, the gestation of most marsupials is characteristically short. However, marsupial pregnancy includes a stage shortly before parturition hypothesized to be homologous to the one in which implantation occurs in eutherians (Hughes, 1974; Harder et al., 1993; Griffith et al., 2017). At this stage, the shell coat surrounding the embryo has been dissolved and cellular contact between the trophoblast and endometrium is established. Following shell coat hatching, the uterine epithelium transforms in a way resembling the peri-implantation epithelial response in eutherians (Laird et al., 2014), although this transformation appears to primarily function in histotrophy rather than attachment (Griffith et al., 2019; Stadtmauer, Basanta et al., 2024). The opossum *Monodelphis domestica* has a gestation of 14.5 days from copulation to parturition (Mate et al., 1994), during the first 11 of which the fetus is surrounded by a proteinaceous shell coat and is fed by maternal uterine secretions (Zeller & Freyer, 2001).

We used single-cell transcriptomics to characterize the endometrial changes at early implantation in two rodent species, the mouse and guinea pig, in comparison with two time points during the short gestation of the marsupial *Monodelphis domestica*, which lacks implantation. In all three species, we targeted the stage when the pre-implantation embryo is a blastocyst, and maternal serum progesterone is elevated: 4.5 dpc for the mouse (Virgo and Bellward, 1974), 6.5 dpc for the guinea pig (Challis et al., 1971), and two stages of the opossum: 7.5 dpc, when the fetus is still a blastocyst (equivalent to the pre-implantation blastocyst in rodents) surrounded by the soft shell coat (Hinds et al., 1992; Yoshida et al., 2019), and day 13.5 of gestation, when the shell coat surrounding the fetus is lost and inflammatory attachment has begun **(Figure 1)**. To identify implantation-specific changes, we also sequenced the non-pregnant uterus from mouse diestrus and guinea pig luteal phase - cycle stages also characterized by high progesterone - and the non-pregnant, non-cycling opossum endometrium. We test for a conserved cellular signature of endometrial receptivity in eutherian species, and look for its equivalent in the opossum, and find that the opossum uterus already presents some of the hallmarks of eutherian implantation at the blastocyst-stage. We analyze time-matched preimplantation blastocysts in these species, and find that gene expression and signaling potential of the fetal trophectoderm shows striking evolutionary conservation despite the considerable divergence of the eutherian implantation mode. Lastly, we compare signaling gene expression of the peri-implantation uterine epithelium to the trophoblast of the fully-developed

placenta, finding considerable overlap which may contribute to tissue stability after loss of the luminal epithelium in invasive placentation. Together, we characterize conserved and divergent characteristics of mammalian implantation and identify possible constraints to the evolution of implantation due to the disruption of maternal tissue integrity during eutherian placentation.

Results

We generated single-cell sequencing libraries from the non-pregnant and peri-implantation endometrium of mouse, guinea pig and opossum **(Figure 2a-b)**, and generated cross-species integrated **(Figure 2c)** and species-specific **(Figure 2d)** two-dimensional embeddings using Uniform Manifold Approximation and Projection (UMAP). We annotated clusters into putative cell types using marker gene identification and refined annotations using the results of non-negative matrix factorization (cNMF) **(Figure S1)** and SAMap homology inference **(Figure S2)**.

Cell type inventories were highly similar between the rodents and opossum **(Figure 2d)**. In all three species, the non-pregnant uterus is predominantly composed of fibroblasts and smooth muscle cells, which make up more than 60% of captured cells **(Figure 2b)**. Relative cell type abundance diverged, however, at the peri-implantation stage. In our rodent species, uterine epithelial cells make up less than 10% of all cells, whereas in the opossum, more than 50% of all cells captured are epithelial at days 7.5 and 13.5 **(Figure 2b)**. This coincides with a pronounced expansion of the uterine glands in the second half of opossum gestation (Harder et al., 1993).

The opossum epithelium expresses some hallmark receptivity genes at the blastocyst stage but differs in expression dynamics

We first explore the similarity between rodent and opossum epithelial cell type composition and gene expression **(Figure 3a, see also Figure S2).** The mouse luminal epithelium displays the distinctive expression of *Ihh*, *Wnt7a*, *Wnt7b* and *Lrg5* (Seishima et al., 2019), as well high levels of *Tacstd2*, epithelial splicing regulatory proteins *Espr1* and *Espr2* (Hayakawa et al., 2017), and the transcription factors *Ehf* (Luk et al., 2018), *Msx1*, and *Klf5* **(Figure 3b)**. The guinea pig luminal epithelial cells express many of the same markers with the exception of *TACSTD2* **(Figure 3b)**. Opossum luminal epithelium includes one cluster enriched for *OAT* (Ornithine Aminotransferase, LE-OAT) and another enriched for *SLCO2A1*+ and *PTGS2*+ (Stadtmauer, Basanta et al., 2024). *OAT*+ luminal epithelial cells were transcriptomically more similar to mouse and guinea pig luminal epithelium (SAMap score of around 0.6) than *SLCO2A*1+ cells **(Figure 3a)**. In the opossum luminal epithelium, the expression of *IHH*, *LGR5*, *LIF* and *MSX2* was only detectable at the blastocyst stage (**Figure 3b)**.

Glandular epithelial gene expression is well conserved across species and across stages **(Figure 3a; Figure S2**; SAMap score ≥ 0.8 in all pairwise combinations). Mouse glandular epithelium is characterized by the expression of *Foxa2*, serine proteases *Prss28* and *Prss29* (Dhakal & Spencer, 2021), *Spink1*, *Guca2b*, *Ltf* and *Sprr2f*. Conserved genes for the glandular epithelium across mouse and guinea pig included *FOXA2*, *ELAPOR1*, *PAX8*, *WWC1*, *MSX1*, *MSX2*, *WFDC2*, *EHF*, *KLF5*, *ESRP1/2* and *ST14* **(Figure 3b).** The opossum's glandular epithelium is also highly similar to that of the rodents, sharing the expression of *ELAPOR1*, *PAX8*, *WWC1*, *MSX1*, *MSX2*, *SOX9*, *PROM1*, *EPCAM*, *WWC1* and ST*14* **(Figure 3b).** *FOXA2* expression was higher in glands at the opossym blastocyst stage. Ciliated epithelial cells (CE) were also identified in the opossum, expressing markers of human ciliated cells (*FOXJ1* and *ADGB*; Garcia-Alonso et al.,

2021), and with greatest SAMap affinity to glandular cells in the mouse and guinea pig (**Figure 3a**) even though there are no glandular ciliated cells in either species.

In the opossum, the abundance of ciliated cells (CE) and a specific luminal epithelial subpopulation (LE-SLCO2A1) increases towards mid-gestation. *OAT*$^{+}$ cells were enriched in the non-pregnant and day 7.5 stages, and *SLCO2A1*$^{+}$ cells were enriched on day 13.5. However, the most drastic change involves the increased abundance of glandular epithelial cells **(Figure 3c).**

In the mouse glandular epithelium *Foxa2, Prss28*, *Prss29*, *Guca2b* and *Spink1* showed higher expression at peri-implantation relative to diestrus, whereas *Lft*, *Sprr2f*, and *Spink12* showed decreased expression at peri-implantation **(Figure 3d)**. *Sprr2f* responds to circulating estrogen levels during the mouse's estrus cycle (Contreras et al., 2010), and it is up-regulated in the uteri of mouse with uterine-specific deletion of *Msx* genes (Sun et al., 2016). *Ltf* is a uterine epithelial-secreted protein also regulated by estradiol, required for both epithelial and stromal *Esr1* expression (Furuminato et al., 2023). Together, these expression dynamics indicate that uterine glands shift from an estrogen- to progesterone-dominated gene expression pattern at the time of implantation.

Genes upregulated in the opossum glandular epithelium at blastocyst-stage relative to non-pregnant, non-cycling stage showed substantial overlap with gene sets generated from experimental perturbations on cell lines and animal models available in the NCBI GEO repository **(see Methods)**. These included categories such as "estradiol mouse BAL cells" (GDS2562), "17beta-estradiol mouse uterus" (GDS1058), and "estradiol mouse uterus" (GSE23241) **(Figure 3e)**. The upregulation of estrogen-responsive genes in the glands at the opossum blastocyst stage constitutes a key difference with respect to the expression dynamics of mouse implantation, which shows an estradiol-progesterone shift. In addition, these results are consistent with the hypothesis that the suppression of estrogen signaling during implantation is a derived attribute of eutherian reproduction (Marinić et al., 2021).

In contrast, genes upregulated in the uterine glands of opossum at the 13.5 dpc placentation stage were enriched for genes stimulated by interleukin-1 (GDS2472; GDS4595), interleukin-15 (GSE59185), interleukin-10 (GSE59148), and interleukin-17A (GDS4601) **(Figure 3e).** This suggests that the inflammatory signaling in opossum late gestation also acts on the glands, consistent with a modulatory effect of inflammation on histotrophic activity of the mother.

Rodent stroma shows greater cell heterogeneity and proliferation at peri-implantation

Mouse fibroblasts separated into three transcriptomically distinct populations associated with different histological microenvironments: subepithelial, inner stromal, and myometrial tissue fibroblasts **(Figure 4a)**, consistent with previous studies of peri-implantation mouse endometrium (Kirkwood et al., 2021). All three populations express *Pdgfra*, *Hoxa9*, *Hoxa10*, *Hoxa11*, and *Pgr*. We identified subepithelial fibroblasts (ESF_subepi) by their enriched expression of *Angptl7*, *Aspg*, and *Ptch2*. Fibroblasts in the inner stroma (ESF_inner) are characterized by enriched expression of *Hand2*, whereas fibroblasts close to the myometrium (TF), also referred to as "tissue fibroblasts", are enriched for *Fbln1*, *Mmp3*, *Lum*, *Ecm1*, *Clec3b*, and *Fap* **(Figure 4b)**.

Guinea pig endometrial fibroblasts clustered into three sub-populations as in the mouse, with high SAMap scores between the corresponding clusters of the two species **(Figure 4a, see Figure S2)**. All endometrial stromal fibroblasts share expression of *PDGFD* and its receptor *PDGFRA*, *HOXA11*, and *SERPINF1*. Tissue fibroblasts express *LUM*, *FBLN1*, *ECM1*, *CLEC11A*, and *DPT* **(Figure 4b)**.

Opossum fibroblasts segregated into only two cell populations, *SMOC2*-positive endometrial stromal (ESF-SMOC2) and *FBLN1*-positive tissue fibroblasts (TF-FBLN1) (Stadtmauer, Basanta et al., 2024). Eutherian endometrial stromal fibroblasts respond to hormonal changes and differentiate into decidual cells. The opossum endometrial stromal fibroblasts show high similarity to eutherian endometrial fibroblasts **(Figure 4a)**, both clusters sharing the expression of *HOXA11* and *PGR*, despite the inability of the opossum's stroma to decidualize (Kin et al., 2014; Erkenbrack et al., 2018). A notable difference between rodent stromal fibroblasts and the opossum's was the lack of significant levels of *HAND2* expression, as well as lower levels of *HOXA* transcription factors **(Figure 4b)**.

Mouse and guinea pig endometrial inner stromal fibroblasts include a subpopulation characterized by numerous proliferation markers. These proliferating stromal cells increased in abundance at the rodent peri-implantation stages **(Figure 4c)** and were absent in the mid and late-gestation opossum endometrium. Finally, there were no substantial differences between the stromal fibroblast gene expression of opossums during mid and late-gestation stages, besides a precipitous decline in abundance **(Figure 4d)**, suggesting that stromal transformation is not involved in attachment or endometrial recognition of pregnancy in the opossum as it is in deciduate (placental) mammals.

Main eutherian implantation signals are present in the opossum epithelial-stromal crosstalk before egg-shell rupture

We inferred maternal cell communication potential from cell type transcriptomes **(see Methods; Figure S3)** and assessed putative cell-cell communication at the epithelial-stromal crosstalk. Then, we explored differential signaling from epithelium to the stroma between the peri-implantation phase and non-pregnant stages in rodents, as well as between days 7.5 and 13.4 and non-pregnant stage in the opossum **(Figure 5)**.

In mouse and guinea pig luminal uterine epithelium, *IHH* was inferred to signal to stromal fibroblasts **(Figure 6a-b)**. In the mouse, *Ihh* signaling was not significantly upregulated at peri-implantation compared to diestrus but the Ihh-receptor complexes *Boc_Ptch1* (2.78-fold, $p = 1.6 \times 10^{-9}$) and *Cdon_Ptch1* (2.64-fold, $p = 4.2 \times 10^{-3}$) were **(Table S1.1)**. In the guinea pig, we found the opposite trend: *IHH* displayed a 2.41-fold upregulation of the ligand at peri-implantation relative to diestrus ($p = 0.06$), but not its receptor complexes *BOC_PTCH1* ($p > 0.1$) or *CDON_PTCH1* ($p > 0.1$) **(Table S1.2)**.

IHH was detected in the glandular epithelium of the opossum at 7.5 dpc **(Figure 6c)**, showing a significant increase from the non-pregnant, non-cycling state to 7.5 dpc (7.11-fold, $p = 8.67 \times 10^{-7}$) **(Table S1.3)**. In the placentation phase at 13.5 dpc, glandular *IHH* expression is reduced to near-zero, suggesting that its expression is limited to a narrow window around the blastocyst stage. With respect to the potential for epithelial-stromal *IHH* signaling in this species, *PTCH1* is highly expressed in opossum endometrial stromal fibroblasts (180.0 TPM), but its co-receptors *BOC* (no ortholog identified), *CDON* (4.6 TPM), and *GAS1* (2.0 TPM) are not, leading the receptor complex to be called as "off" in our cell communication inference analysis **(Figure 6c)**. However, given the expression of both the ligand and its main ligand-binding receptor subunit in opossum, we suggest that this active signaling pathway may be conserved across therians, although experimental verification will be necessary.

Leukemia inhibitory factor (*LIF*) signaling from glandular and to a lesser extent luminal epithelium was detected in the mouse, where *Lif* production showed nominal upregulation in epithelial cells on day 4.5 versus diestrus (1.87-fold increase, $p = 0.35$) **(Table S1.1).** The guinea pig,

in contrast, lacked luminal or glandular epithelial *LIF* expression, and therefore signaling via this pathway was not inferred **(Figure 3b; Figure 6b)**. *LIF* expression can rescue implantation in mice under low-estradiol conditions (Chen et al., 2000), suggesting that it mediates estrogen signaling, a function that may not be needed in the guinea pig. In the opossum, *LIF* signaling from the luminal epithelium to the stroma was present at day 7.5, but reduced in magnitude (7.7-fold decrease, $p = 5.1 \times 10^{-6}$) compared to the expression in the non-pregnant stage and not expressed at day 13.5 **(Figure 6c-d)**. These data suggest that LIF signaling to the stroma is not related to endometrial recognition of pregnancy in opossum **(Table S1.4).**

In mouse peri-implantation, we identified potential epithelial *Wnt7a*, *Wnt7b*, and *Wnt11* signaling from the epithelium to the stroma via frizzled receptors *Fzd1*, *Fzd2* and *Fzd3* **(Figure 6a)**. For the signaling involving *Wnt7b*, the receptor *Fzd1*, along with several secreted frizzled related proteins (SFRPs), were significantly upregulated during implantation compared to diestrus **(Table S1.1)**. In guinea pig peri-implantation, we identified *WNT7B* signaling from luminal epithelium to the glands **(Figure 6b)**. In the non-pregnant opossum, *WNT5A, WNT7A, WNT7B,* and *WNT11* were expressed (>20% of cells in the cluster) in luminal epithelium, but were downregulated below our expression threshold at day 7.5 (*WNT7A* $p = 3.68 \times 10^{-11}$; *WNT7B*: p=0.022; *WNT11*: $p = 1.38 \times 10^{-23}$ *WNT5A*: $p=6.96 \times 10^{-13}$) compared to the non-pregnant **(Table S1.3)**, and remained off at day 13.5 **(Table S1.4)**. In summary, rodent uterine epithelium expresses peri-implantation Wnt signaling which is absent in the opossum **(Figure 6c-d)**.

Blastocyst signaling is conserved across Theria

To complement uterine signaling, we assessed the putative signaling between the blastocyst and uterine epithelium in mouse, human, and opossum, utilizing published blastocyst expression data on opossum E7.5 bilaminar blastocyst (Mahadevaiah et al., 2020), mouse E4.5 (Nakamura et al., 2015), guinea pig E5.5 (Guan et al., 2024), and human day 7 (Petropoulos et al., 2016). In addition, we included data from the human endometrial mid-secretory epithelium (Marečková et al., 2024).

We first inferred and investigated the potential signaling between the trophoectoderm and the maternal epithelium. We found that in all four species, the trophectoderm shows potential to signal to the maternal epithelium by Wnt ligands. In the mouse, these include *WNT3A, WNT6, WNT7B,* and *WNT9A* **(Figure 7a)**. Human data suggests trophectoderm signaling to the luminal epithelium via *WNT3, WNT5B, WNT6, WNT7A,* and *WNT7B* **(Figure 7b)**. In the guinea pig, it included *WNT6* and *WNT3* **(Figure 7c)**. In opossum, blastocyst-expressed Wnt ligands with epithelial uterine receptors included *WNT3A, WNT6, and WNT11* **(Figure 7d)**. Interestingly, in the opossum, the Wnt signaling had concomitant receptors in the glandular instead of the luminal epithelium. The trophectoderm of the four species also expressed BMP family ligands, including *BMP8A* in the mouse, *BMP8A*, *BMP4* and *BMP2* in human, and *BMP4* and *BMP2* in the opossum **(Figure 7)**.

Signaling by *IL6*, a trophectoderm marker involved in signaling to the inner cell mass (Plana-Carmona et al., 2022), *LIF* (Cullinan et al., 1996) and *IGF2* (Rappolee et al., 1992) was not conserved: whereas *IL6* was inferred to signal to the luminal epithelium only in the human, *LIF* was detected only in the rodents, and *IGF2* only in mouse trophectoderm **(Figure 7a-c)**. Expression of growth differentiation genes such as *GDF11* was unique to eutherians.

We then explored conservation of blastocyst gene expression. Enzymes involved in steroid biosynthesis in the blastocyst also showed conservation across species, including dehydrogenase enzymes involved in cholesterol metabolism and estrogen synthesis such as *HSD17B7*, *HSD17B11* and *HSD17B12* (Luu-The et al., 2006; Prehn et al., 2009) **(Figure 8a)**. Blastocyst-secreted proteases function in implantation to digest the layers covering the embryo (Salamonsen & Nie, 2002; Denker & Tyndale-Biscoe, 1986; Selwood, 2000). Trophectoderm protease expression was found to be

highly conserved across the marsupial, rodent, and primate species, including *ADAM* family genes and cathepsins **(Figure 8b)**. This suggests that protease expression in the extraembryonic membranes is conserved among therian mammals (including marsupials) at the blastocyst stage.

The conserved presence of protease expression in the trophectoderm from opossums to humans is thought to elicit a maternal response at implantation characterized by cellular stress (Brosens et al., 2014; Erkenbrack et al., 2018) and inflammation (Griffith et al., 2017). We investigated the degree to which the uterus at peri-implantation appeared to respond to signaling from the embryo in this way. Day 7.5 of opossum gestation shows an increase in abundance of inflammatory immune cells (PMN) that is maintained at day 13.5 **(Figure 8c)**. The opossum inflammatory attachment reaction has been reported to be characterized by expression of *IL1A, IL6, IL10, IL17A, CXCL8,* and *TNF* (Griffith et al., 2017; Hansen et al., 2017). However, few of these were upregulated in our rodent samples at implantation, although the number of macrophages captured increased **(Figure 8d)**. However, differential gene expression analysis of macrophages between diestrus and peri-implantation in the mouse showed upregulation of genes such as *Clec4d*, *Il1r2*, *Il1rn*, *Cxcl1*, *Cxcl2* and *Lif*, suggesting a transition in macrophage polarization towards a pro-inflammatory profile **(Figure 8e)**. We have also previously reported that some inflammatory mediators are expressed by the 13.5 dpc opossum placenta are produced by the syncytial trophoblast **(Figure 8d)** (Stadtmauer & Wagner, 2020b; Chavan et al., 2021; Stadtmauer, Basanta et al., 2024). From these comparisons, it is unclear that trophectoderm expression of proteases at peri-implantation is associated with an inflammatory response. A study of post-attachment stages would be required to resolve this question with greater precision.

The post-implantation interface maintains signaling continuity by cell type substitution

Paracrine interactions between maternal cell types are critical for the establishment and maintenance of pregnancy. These interactions include the remodeling of endothelial cells and the regulation of immune cells. We traced the conservation of signaling between four major functional cell type classes - epithelial, stromal, macrophage, and endothelial cells - between mouse and guinea pig peri-implantation and the opossum 7.5 and 13.5 dpc stages, and how these interactions change later in pregnancy after the stroma and epithelium are remodeled.

Luminal epithelium in all species expressed high levels of vascular endothelial growth factor (*VEGF*) and placental growth factor (*PGF*), pro-angiogenic ligands for the endothelial cell receptor *FLT1* (Ribatti, 2008) **(Figure 9a; Table S2)**. Macrophages demonstrated signaling to endothelial cells via *IGF1* and *TNF* in mouse, guinea pig, and 7.5 dpc opossum (**Figure 9a**). Signaling from macrophages to stromal cells included *TNF* and *TGFB1* (**Figure 9a**). Signaling from the stroma to the epithelium included *BMP2* and *IGF1* in rodents and opossum **(Figure 9a; Table S2.3-4)**. Stromal-to-macrophage signaling included *CXCL12* and prostaglandin E2 via the synthase *PTGES3* in both rodents and the opossum **(Figure 9a; Table S2.1-2)**.

The development of the invasive fetal-maternal interface involves a major change in constituent cell types present in the endometrium: the luminal epithelium is eroded and replaced by the trophoblast, and endometrial stromal fibroblasts differentiate into decidual stromal cells **(Figure 9a)**. To understand how the roles of single cell types change in this tissue restructuring, we first compared the expression of secreted ligands between endometrial stromal fibroblasts at the rodent peri-implantation period to the decidual ligands of the established fetal-maternal interface (Stadtmauer, Basanta et al., 2024). Considerable divergence of secreted signaling was found between mid-gestation decidual cells and their developmental precursors in peri-implantation mouse (Jaccard

similarity index = 0.36 in the range from 0-1) as well as in guinea pig (Jaccard index = 0.48 for PRL+ decidual cells, 0.53 for OXT+ decidual cells) **(Figure 9b; Table S3)**.

We predicted that the successful establishment of pregnancy, which involves a physical replacement of maternal luminal epithelium by the trophoblast in eutherian mammals, may require a continuity of epithelial signaling interactions. Using data from our previous study (Stadtmauer, Basanta et al., 2024), we calculated Pearson correlations between the secreted ligands repertoires of mid-gestation cell types with the uterine epithelium of blastocyst attachment stage mouse, guinea pig, and opossum. In all three species, integrated trophoblast cell types were among the most similar in their secreted ligands to the uterine epithelium **(Figure 9c)**. In the mouse, invasive trophoblast giant cells (glycogen and spiral artery-remodeling) had greater epithelial similarity than non-invasive (canal and sinusoidal). In the guinea pig, subplacental cytotrophoblast showed greater similarity to uterine epithelial cells, and in the opossum, cytotrophoblast is most similar to uterine epithelium (**Figure 9c-d)**.

We compared the overlapping ligands between the top-scoring placental cell types resulting from the Pearson correlation and the peri-attachment epithelium ligands **(Table S4)**. In all species, the set of ligands produced by invasive trophoblast was smaller than those produced by the peri-implantation epithelium. Among the non-overlap, epithelial-specific ligands in mouse included receptivity markers such as *IHH, WNT*, and *LIF* and trophoblast-specific ligands included *BMP8A* and *IGF2* **(Figure 10a)**. In the guinea pig, *IHH* and *WNT* are unique to the epithelium, *LEP* and *OXT* to the extraplacental trophoblast and *GDF15* to the subplacental cytotrophoblast **(Figure 10b)**. In the opossum, *BMP8A* and *IHH* were also cytotrophoblast and epithelium specific respectively. The syncytiotrophoblast expressed inflammatory mediators as mentioned above **(Figure 10c)**. In humans, the extravillous trophoblast expresses *LEP* and *IGF2* and the epithelium *IHH*, *WNT* and *LIF* **(Figure 10d)**. Because of the relationship between invasive trophoblast subtypes and vascular remodeling, we next tested what proportion of the overlapping ligands between the epithelium and the top-scoring trophoblasts subtypes is involved in vascular interactions, that is to say, which ligands have receptors in the vasculature. Among the overlapping ligands between epithelium and the top-scoring trophoblast match in rodents, a substantial portion of ligands had expressed receptors in vascular cell types of endothelial cells and pericytes. In the mouse, these included *ANGPT2*, *HDGF*, stem cell factor *KITLG*, *VEGFA*, *VEGFB*. In the guinea pig, the vascular growth factors *VEGFA, VEGFB, VEGFC, PENK, VWF* and stem cell factor *KITLG*. We found that in rodents a substantial percentage of the overlapping ligands had indeed receptors in the vasculature (51% and 40% in mouse and guinea pig respectively). A considerable percentage was also in the opossum, falling slightly behind the rodents with 37.5% of the shared ligands having concomitant receptors in the vasculature (**Figure 10e)**. Overall, the pattern suggests that in rodents the trophoblast takes over part of the luminal epithelial signaling function, and that the ability to substitute for the epithelium was an ancestral feature of the therian trophoblast which may enable its loss in invasive placentation.

Discussion

Embryo implantation constitutes the most intimate and specialized cellular contact between the embryo and the mother. This first contact is essential in eutherians to establish the placenta and initiate stable gestational development. We compared two rodent species and examined the evolutionary conservation of the eutherian implantation uterine response in contrast with the opossum, which lacks implantation and a prolonged gestation period. This comparison reveals insights into the evolutionary origins of implantation.

Knowledge of expression patterns and signaling crosstalk during implantation largely derives from studies on mice (Hantak et al., 2014; Yang et al., 2021), with limited molecular information from other rodent species (Blandau, 1949; Enders & Schlafke, 1969; Cha & Dey, 2015). As mouse and guinea pig are phylogenetically distant, with the common ancestor being Rodentia's most recent common ancestor, including the guinea pig in our analysis helped to provide broader insight into rodent reproductive biology. The structure and cell biology of the placental interface established later in pregnancy differ substantially between mouse and guinea pig (Stadtmauer, Basanta et al., 2024). At the implantation stage, however, we found a broadly conserved implantation biology between the two species in cell-type composition, gene expression in individual cell types and cell-cell communication.

We generated single-cell atlas of the implantation and non-receptive endometrium of mouse and guinea pig, as well as the non-pregnant, mature blastocyst, and placental attachment stages of the gray short-tailed opossum *Monodelphis domestica*. This marsupial has been established as an outgroup species to eutherians and used to infer the reproductive changes that evolved with eutherian embryo implantation (Griffith et al., 2017). The endometrium of opossum consisted of largely homologous cell types to that of mouse and guinea pig, we observed greater epithelial cell heterogeneity in the opossum and greater stromal cell diversity in rodents, suggesting that the divide between hemotrophic and histotrophic biologies in marsupials and eutherians is represented at the level of cell type diversity. Further research will be required to determine whether the pregnancy-specific differentiation of the opossum luminal epithelium to a secretory state enriched in late pregnancy (LE-SLCO2A1), with lower SAMap mapping scores to mouse and guinea pig luminal epithelium, represents an evolutionarily novel cell type in marsupials. Likewise, opossum *FOXJ1*$^{+}$ ciliated epithelial cells (CE) had no equivalent in mouse and guinea pig, as in these species ciliated epithleium is restricted to the oviduct, unlike in humans, which also have ciliated uterine epithelial cells (Hunter et al., 2024). Further comparative research of oviductal epithelium from more species will be required to assess whether this cell type evolved independently in marsupials and eutherians.

The dynamics of cell type abundance in response to hormonal changes also differed vastly between marsupials and eutherians. In *Monodelphis domestica*, the subepithelial stroma undergoes remodeling during the first 7 days of pregnancy, wherein endometrial fibroblasts that are abundant in the non-pregnant uterus are replaced by uterine glands, which produce histotrophic nutrition for the offspring (Griffith et al., 2019). While glands predominate within the endometrium of the opossum after 7.5 dpc, the stroma dominates in abundance in rodents and shows a parallel regional differentiation into subepithelial, inner stromal, and myometrial populations in both mouse and guinea pig. Given the supportive role of uterine glands in marsupials, the shift from glands to the stroma as a major source of support for the embryo has likely been one of the essential steps in the evolution of eutherian implantation.

It is not straightforward to identify homologous stages between the opossum's short gestation and that of eutherians based on transcriptional similarity. Denker & Tyndale-Biscoe (1986) used "(superficial) implantation" to refer to the specialized cellular contact between extraembryonic membranes and endometrium which occurs before parturition in macropodid marsupials such as kangaroos and wallabies. In the opossum, this would apply to the day 12-13.5 of pregnancy. Furthermore, inflammatory cytokine expression during the last two days of opossum gestation has been proposed as homologous to inflammation during eutherian implantation (De Filippo et al., 2013; Hendriks et al., 2008; Griffith et al., 2017). For this reason, it is surprising that our comparative analysis shows greater similarity of rodent pre-implantation (mouse 4.5 dpc, guinea pig 6.5 dpc) to the blastocyst stage of opossum (day 7.5 dpc; blastocyst stage) than to placentation (13.5 dpc). We find that during this window, *IHH*, *WNT7A*, and *MSX2* are expressed, along with the glandular epithelial expression of *FOXA2* and the serine protease *ST14*. These timepoints share

additional similarities in embryonic staging (summarized in Malkowska et al., 2022) and elevated circulating progesterone **(Figure 1)**. Indeed, some of these genes, such as *IHH*, are progesterone-responsive (Matsumoto et al., 2002), suggesting that this window of similarity may represent a uterine response to hormonal changes of early pregnancy. The 7.5 dpc stage of opossum pregnancy is also, like the implantation window of humans (Muter et al., 2023), the period when pregnancy failure is most likely to occur (Yoshida et al., 2019). Wnt signaling, on the other hand, was found to be expressed in non-cycling opossum endometrium but not at either pregnant timepoint. This suggests that prolonged epithelial Wnt signaling is likely a derived component of the eutherian implantation process. Together, these results demonstrate that the expression of some of the signaling pathways that were already functional in the uterus of the last common ancestor of marsupials and eutherians were later recruited into eutherian implantation.

We found high conservation of gene expression between the blastocyst trophectoderm of the opossum, rodents, and the human, including proteases, steroid biosynthetic enzymes, and Wnt and BMP ligands with receptors expressed in the endometrium. Conservation suggests that the signaling potential of the blastocyst has not undergone dramatic change in therian evolution, and as a result we must attribute major changes underlying the innovation in implantation mode in eutherians to changes in the maternal tissue. Elucidation of precisely what these maternal innovations were is a deserving focus of future investigation. That said, one source of fetal evolutionary change despite strong conservation is neo-functionalization of ancestral trophectoderm products such as proteases, which presumably lost their functional necessity for hatching once the shell coat was evolutionarily lost in stem eutherians (Selwood, 2000). Serine proteases have been reported to function in matrix dissolution to aid placental invasion (Salamonsen & Nie, 2002) and in embryo screening (Brosens et al., 2014), two functions which likely diverge from their ancestral role.

Comparison of the secreted signaling repertoire of the uterine epithelium at the peri-implantation stage and the trophoblast at mid-gestation revealed continuity of interactions throughout pregnancy. Our results suggest that eutherian implantation is a transition in tissue composition, where the luminal epithelium is replaced by the trophoblast, forming a meta-stable tissue configuration: the maternal-fetal interface (Pavlicev & Wagner, 2024). The high similarity between the signaling repertoires of trophoblast and uterine epithelium indicates that the trophoblast is uniquely capable of mediating this transition. The opossum, which lacks decidualization and epithelial erosion during placentation, nevertheless showed overlap of cytotrophoblast secreted signaling with its uterine luminal epithelium, suggesting that this substitution capacity reflects a conserved epithelial nature of the therian trophoblast. Redundancy between trophectoderm and epithelial signaling may have allowed the transition to invasive forms of placentation to evolve in the stem eutherian lineage without greater disruption to endometrial signaling networks.

Altogether, our data indicate that hallmarks of the eutherian endometrial receptivity - specifically pre-implantation changes to the luminal epithelium - are shared between rodents and the opossum and thus predate the origin of invasive implantation in placental mammals. This suggests that necessary cell-biological prerequisites for eutherian invasive implantation may have existed in the therian common ancestor, prevented by the presence of the shell coat which prevents direct trophoblast-uterine contact until late gestation; thus, the loss of this membrane thus may have precipitated major changes in placentation and reproductive mode in the eutherian lineage. Further comparative research is needed to clarify this sequence of evolutionary events and to reconcile it with the hypothesis that post-hatching cell-cell contact is the marsupial homolog to the eutherian implantation stage.

Acknowledgements

The authors thank the Yale Center for Genomic Analysis (NIH 1S10OD030363-01A1) for library preparation and use of their high-performance computing cluster.

Funding

This research was funded by the Austrian Science Fund (FWF) #33540 to MP, the John Templeton Foundation (#61329) to GPW, and the Yale Institute for Biospheric Studies Early Grant to DJS. DJS was supported by a training grant from the National Institutes of Health (T32 GM 007499). GPW receives research support from the Hagler Institute of Advanced Studies at Texas A&M University.

Author contributions

Conceptualization: GPW, MP
Funding acquisition: GPW, MP, DJS
Experimentation: SBM, DJS, JDM, CMG, AGC
Animal Colony Maintenance: SBM, DJS, JDM, GD
Data analysis: SBM, DJS
Supervision: GPW, MP
Writing - original draft: SBM, DJS
Writing - review & editing: SBM, DJS, GPW, MP

Citations

Blandau, R. J. (1949). Embryo-endometrial interrelationship in the rat and guinea pig. *The Anatomical Record, 104,* 331-359.

Brosens, J.J., Stalker, M.S., Teklenburg, G., et al. (2014) Uterine selection of human embryos at implantation. *Scientific Reports,* 4, 3894.

Carter, A. M. (2007). Animal models of human placentation–a review. *Placenta, 28,* S41-S47.

Cha, J. M., & Dey, S. K. (2015). Reflections on rodent implantation. *Regulation of Implantation and Establishment of Pregnancy in Mammals: Tribute to 45 Year Anniversary of Roger V. Short's" Maternal Recognition of Pregnancy*", 69-85.

Challis, J. R. G., Heap, R. B., & Illingworth, D. V. (1971). Concentrations of oestrogen and progesterone in the plasma of non-pregnant, pregnant and lactating guinea-pigs. *Journal of Endocrinology, 51*(2), 333-345.

Chavan, A. R., Griffith, O. W., Stadtmauer, D. J., Maziarz, J., Pavlicev, M., Fishman, R., Koren L., Romero R., & Wagner, G. P. (2021). Evolution of embryo implantation was enabled by the origin of decidual stromal cells in eutherian mammals. *Molecular biology and evolution, 38*(3), 1060-1074.

Chen, J. R., Cheng, J. G., Shatzer, T., Sewell, L., Hernandez, L., & Stewart, C. L. (2000). Leukemia inhibitory factor can substitute for nidatory estrogen and is essential to inducing a receptive uterus for implantation but is not essential for subsequent embryogenesis. *Endocrinology, 141*(12), 4365-4372.

Contreras, C. M., Akbay, E. A., Gallardo, T. D., Haynie, J. M., Sharma, S., Tagao, O., Bardeesy, N., Takahashi, M., Settleman, J., Wong, K., & Castrillon, D. H. (2010). Lkb1 inactivation is sufficient to drive endometrial cancers that are aggressive yet highly responsive to mTOR inhibitor monotherapy. *Disease models & mechanisms, 3*(3-4), 181-193**.**

Cullinan, E. B., Abbondanzo, S. J., Anderson, P. S., Pollard, J. W., Lessey, B. A., & Stewart, C. L. (1996). Leukemia inhibitory factor (LIF) and LIF receptor expression in human endometrium suggests a potential autocrine/paracrine function in regulating embryo implantation. *Proceedings of the National Academy of Sciences, 93*(7), 3115-3120.

Deanesly, R. (1960). Implantation and early pregnancy in ovariectomized guinea-pigs. *Reproduction, 1*(3), 242-248.

Denker, H. W., & Tyndale-Biscoe, C. H. (1986). Embryo implantation and proteinase activities in a marsupial (Macropus eugenii) Histochemical patterns of proteinases in various gestational stages. *Cell and tissue research, 246,* 279-291.

Denker, H. W. (1993). Implantation: a cell biological paradox. *Journal of Experimental Zoology, 266*(6), 541-558.

Dey, S. K., Lim, H., Das, S. K., Reese, J., Paria, B. C., Daikoku, T., & Wang, H. (2004). Molecular cues to implantation. *Endocrine reviews, 25*(3), 341-373.

Dhakal, P., & Spencer, T. E. (2021). Generation and analysis of Prss28 and Prss29 deficient mice using CRISPR□Cas9 genome□editing. *Molecular reproduction and development, 88*(7), 482-489.

Enders, A. C., & Schlafke, S. (1969). Cytological aspects of trophoblast□uterine interaction in early implantation. *American Journal of Anatomy, 125*(1), 1-29.

Erkenbrack, E. M., Maziarz, J. D., Griffith, O. W., Liang, C., Chavan, A. R., Nnamani, M. C., & Wagner, G. P. (2018). The mammalian decidual cell evolved from a cellular stress response. *PLoS biology, 16*(8), e2005594.

Frankenberg, S. R., De Barros, F. R., Rossant, J., & Renfree, M. B. (2016). The mammalian blastocyst. *Wiley Interdisciplinary Reviews: Developmental Biology, 5*(2), 210-232.

Furuminato, K., Minatoya, S., Senoo, E., Goto, T., Yamazaki, S., Sakaguchi, M., Toyotal, K., Iguchi, T., & Miyagawa, S. (2023). The role of mesenchymal estrogen receptor 1 in mouse uterus in response to estrogen. *Scientific reports, 13*(1), 12293.

Garcia-Alonso, L., Handfield, L. F., Roberts, K., Nikolakopoulou, K., Fernando, R. C., Gardner, L., Woodhams, B., Arutyunyan, A., Polanski, K., Hoo, R., Sancho-Serra, C., Li, T., Kwakwa, K., Tuck, E., Kleshchevnikov V., Tarkowska, A., Porter, T., Mazzeo, C.I., van Dongen, S., Dabrowska, M., Vaskivskyi, V., Mahbubani, T., Park, J,., Jimenez-Linan, M., Campos, L., Kiselev, V., Lindskog, C., Ayuk, P., Prigmore, E., Stratton, M.R., Saeb-Parsy, K., Moffett, A., Moore, L., Bayraktar, O.A., Teichmann, S.A., Turco, M.Y., & Vento-Tormo, R. (2021). Mapping the temporal and spatial dynamics of the human endometrium in vivo and in vitro. *Nature genetics, 53*(12), 1698-1711.

Griffith, O. W., Chavan, A. R., Protopapas, S., Maziarz, J., Romero, R., & Wagner, G. P. (2017). Embryo implantation evolved from an ancestral inflammatory attachment reaction. *Proceedings of the National Academy of Sciences, 114*(32), E6566-E6575.

Griffith, O. W., Chavan, A. R., Pavlicev, M., Protopapas, S., Callahan, R., Maziarz, J., & Wagner, G. P. (2019). Endometrial recognition of pregnancy occurs in the grey short-tailed opossum (Monodelphis domestica). *Proceedings of the Royal Society B, 286*(1905), 20190691.

Guan, T., Guo, J., Lin, R., Liu, J., Luo, R., Zhang, Z., Pei, D., & Liu, J. (2024). Single-cell analysis of preimplantation embryonic development in guinea pigs. *BMC genomics, 25*(1), 911.

Hansen, V. L. (2017). *Immunology of the gray short-tailed opossum during pregnancy and prenatal development* (Doctoral dissertation, The University of New Mexico).

Hansen, V. L., Faber, L. S., Salehpoor, A. A., & Miller, R. D. (2017). A pronounced uterine pro-inflammatory response at parturition is an ancient feature in mammals. *Proceedings of the Royal Society B: Biological Sciences*, *284*(1865), 20171694.

Hantak, A. M., Bagchi, I. C., & Bagchi, M. K. (2014). Role of uterine stromal-epithelial crosstalk in embryo implantation. *The International journal of developmental biology*, *58*, 139.

Harder, J.D., & Fleming, M.W. (1981). Estradiol and progesterone profiles indicate a lack of endocrine recognition of pregnancy in the opossum. *Science*, 212, 1400-1402.

Harder, J.D., Stonerook, M.J., & Pondo, J. (1993). Gestation and placentation in two New World opossums: *Didelphis virginiana* and *Monodelphis domestica*. *The Journal of Experimental Zoology* 266, 463-479.

Hayakawa, A., Saitoh, M., & Miyazawa, K. (2017). Dual roles for epithelial splicing regulatory proteins 1 (ESRP1) and 2 (ESRP2) in cancer progression. *Protein Reviews: Volume 17*, 33-40.

Hendriks, J. J., Slaets, H., Carmans, S., de Vries, H. E., Dijkstra, C. D., Stinissen, P., & Hellings, N. (2008). Leukemia inhibitory factor modulates production of inflammatory mediators and myelin phagocytosis by macrophages. *Journal of neuroimmunology*, *204*(1-2), 52-57.

Hinds, L. A., Reader, M., Wernberg-Moller, S., & Saunders, N. R. (1992). Hormonal evidence for induced ovulation in Monodelphis domestica. *Reproduction*, *95*(1), 303-312.

Hughes, R. L. (1974). Morphological studies on implantation in marsupials. *Reproduction*, *39*(1), 173-186.

Hunter, M.I., Thies, K.M., Winuthayanon, W. (2024). Hormonal regulation of cilia in the female reproductive tract. *Current opinion in endocrine and metabolic research*, 34, 100503.

Kin, K., Maziarz, J., & Wagner, G. P. (2014). Immunohistological study of the endometrial stromal fibroblasts in the opossum, Monodelphis domestica: evidence for homology with eutherian stromal fibroblasts. *Biology of reproduction*, *90*(5), 111-1.

Kirkwood, P. M., Gibson, D. A., Smith, J. R., Wilson□Kanamori, J. R., Kelepouri, O., Esnal□Zufiaurre, A., Dobie, R., Henderson, N.C., & Saunders, P. T. (2021). Single□cell RNA sequencing redefines the mesenchymal cell landscape of mouse endometrium. *The FASEB Journal*, *35*(4).

Laird, M. K., Thompson, M. B., Murphy, C. R., & McAllan, B. M. (2014). Uterine epithelial cell changes during pregnancy in a marsupial (Sminthopsis crassicaudata; Dasyuridae). *Journal of Morphology*, *275*(10), 1081-1092.

Lee, K. Y., & DeMayo, F. J. (2004). Animal models of implantation. *Reproduction*, *128*(6), 679-695.

Luk, I. Y., Reehorst, C. M., & Mariadason, J. M. (2018). ELF3, ELF5, EHF and SPDEF transcription factors in tissue homeostasis and cancer. *Molecules*, *23*(9), 2191.

Luu-The, V., Tremblay, P., & Labrie, F. (2006). Characterization of type 12 17beta-hydroxysteroid dehydrogenase, an isoform of type 3 17beta-hydroxysteroid dehydrogenase responsible for estradiol formation in women. *Molecular endocrinology (Baltimore, Md.)*, *20*(2), 437–443.

Machelak, W., Szczepaniak, A., Jacenik, D., & Zielińska, M. (2023). The role of GDF11 during inflammation–An overview. *Life Sciences*, *322*, 121650.

Mahadevaiah, S. K., Sangrithi, M. N., Hirota, T., & Turner, J. M. (2020). A single-cell transcriptome atlas of marsupial embryogenesis and X inactivation. *Nature*, *586*(7830), 612-617.

Malkowska, A., Penfold, C., Bergmann, S., & Boroviak, T.E. (2022). A hexa-species transcriptome atlas of mammalian embryogenesis delineates metabolic regulation across three different implantation modes. *Nature Communications*, 13, 3407.

Marečková, M., Garcia-Alonso, L., Moullet, M., Lorenzi, V., Petryszak, R., Sancho-Serra, C., Oszlanczi, A., Mazzeo, C., I., Hoffmann, S., Krassowski, M., Garbutt, K., Kelaval., I, Gaitskell, K., & Vento-Tormo, R. (2024). An integrated single-cell reference atlas of the human endometrium. *Nature Genetics*, 1-13.

Marinić, M., Mika, K., Chigurupati, S., & Lynch, V. J. (2021). Evolutionary transcriptomics implicates HAND2 in the origins of implantation and regulation of gestation length. *Elife*, *10*, e61257.

Mate, K. E., Robinson, E. S., A. Pedersen, R., & L. Vandeberg, J. (1994). Timetable of in vivo embryonic development in the grey short□tailed opossum (Monodelphis domestica). *Molecular reproduction and development*, *39*(4), 365-374.

Matsumoto, H., Zhao, X., Das, S.K., Hogan, B.L.M., Dey, S.K., 2002. (2002). Indian hedgehog as a progesterone-responsive factor mediating epithelial-mesenchymal interactions in the mouse uterus. *Developmental biology*, 245, 280-290.

Medawar, P. B. (1953). Some immunological and endocrinological problems raised by the evolution of viviparity in vertebrates. *Symposia of the Society for Experimental Biology* 44:320338.

Mess, A., & Carter, A. M. (2006). Evolutionary transformations of fetal membrane characters in Eutheria with special reference to Afrotheria. *Journal of Experimental Zoology Part B: Molecular and Developmental Evolution, 306*(2), 140-163.

Mor, G., Cardenas, I., Abrahams, V., & Guller, S. (2011). Inflammation and pregnancy: the role of the immune system at the implantation site. *Annals of the new York Academy of Sciences, 1221*(1), 80-87

Muter, J., Lynch, V. J., McCoy, R. C., & Brosens, J. J. (2023). Human embryo implantation. *Development, 150*(10), dev201507.

Nakamura, T., Yabuta, Y., Okamoto, I., Aramaki, S., Yokobayashi, S., Kurimoto, K., Sekiguchi, K., Nakagawa, M., Yamamoto, T., & Saitou, M. (2015). SC3-seq: a method for highly parallel and quantitative measurement of single-cell gene expression. *Nucleic acids research, 43*(9), e60-e60.

Osokine, I., Siewiera, J., Rideaux, D., Ma, S., Tsukui, T., & Erlebacher, A. (2022). Gene silencing by EZH2 suppresses TGF-β activity within the decidua to avert pregnancy-adverse wound healing at the maternal-fetal interface. *Cell reports, 38*(5).

Pavlicev, M., & Wagner, G. P. (2024). Reading the palimpsest of cell interactions: What questions may we ask of the data?. *Iscience, 27*(5).

Petropoulos, S., Edsgärd, D., Reinius, B., Deng, Q., Panula, S. P., Codeluppi, S., Plaza Reyes, A., Linnarsson, S., and Lanner, F. (2016). Single-cell RNA-seq reveals lineage and X chromosome dynamics in human preimplantation embryos. *Cell, 165*(4), 1012-1026.

Plana-Carmona, M., Stik, G., Bulteau, R., et al. (2022). The trophectoderm acts as a niche for the inner cell mass through C/EBPα-regulated IL-6 signaling. *Stem Cell Reports 17*(9), P1991-P2004.

Prehn, C., Möller, G., & Adamski, J. (2009). Recent advances in 17beta-hydroxysteroid dehydrogenases. *The Journal of Steroid Biochemistry and Molecular Biology, 114*(1-2), 72-77.

Rappolee, D. A., Sturm, K. S., Behrendtsen, O., Schultz, G. A., Pedersen, R. A., & Werb, Z. (1992). Insulin-like growth factor II acts through an endogenous growth pathway regulated by imprinting in early mouse embryos. *Genes & development, 6*(6), 939-952.

Renfree, M. B. (2000). Maternal recognition of pregnancy in marsupials. *Reviews of Reproduction, 5*(1), 6-11.

Ribatti, D. (2008). The discovery of the placental growth factor and its role in angiogenesis: a historical review. *Angiogenesis, 11*(3), 215-221.

Salamonsen, L. A., & Nie, G. (2002). Proteases at the endometrial–trophoblast interface: their role in implantation. *Reviews in Endocrine and Metabolic Disorders, 3*, 133-143.

Schlafke, S., & Enders, A. C. (1975). Cellular basis of interaction between trophoblast and uterus at implantation. *Biology of reproduction*, *12*(1), 41-65.

Selwood, L. (2000). Marsupial egg and embryo coats. *Cells Tissues Organs*, *166*(2), 208-219.

Seishima, R., Leung, C., Yada, S., Murad, K. B. A., Tan, L. T., Hajamohideen, A., Tan, S.H., Itoh H., Murakami, K., Ishida, Y., Nakamizo S., Yoshikawa, Y., Wong, E., & Barker, N. (2019). Neonatal Wnt-dependent Lgr5 positive stem cells are essential for uterine gland development. *Nature communications*, *10*(1), 5378.

Siriwardena, D., & Boroviak, T. E. (2022). Evolutionary divergence of embryo implantation in primates. *Philosophical Transactions of the Royal Society B*, *377*(1865), 20210256.

Stadtmauer, D.J., & Wagner, G.P. (2020a). The primacy of maternal innovations to the evolution of embryo implantation. *Integrative and Comparative Biology*, 60(3), 742-752.

Stadtmauer, D. J., & Wagner, G. P. (2020b). Cooperative inflammation: the recruitment of inflammatory signaling in marsupial and eutherian pregnancy. *Journal of reproductive immunology*, *137*, 102626.

Stadtmauer, D. J., Basanta Martínez, S., Maziarz, J. D., Cole, A. G., Dagdas, G., Smith, G. R., van Breukelen, F., Pavlicev, M., & Wagner, G. P. (2024). Cell type and cell signaling innovations underlying mammalian pregnancy. *bioRxiv*, 2024-05.

Sun, X., Park, C. B., Deng, W., Potter, S. S., & Dey, S. K. (2016). Uterine inactivation of muscle segment homeobox (Msx) genes alters epithelial cell junction proteins during embryo implantation. *The FASEB Journal*, *30*(4), 1425.

Virgo, B. B., & Bellward, G. D. (1974). Serum progesterone levels in the pregnant and postpartum laboratory mouse. *Endocrinology*, *95*(5), 1486-1490.

Wildman, D. E., Chen, C., Erez, O., Grossman, L. I., Goodman, M., & Romero, R. (2006). Evolution of the mammalian placenta revealed by phylogenetic analysis. *Proceedings of the National Academy of Sciences*, *103*(9), 3203-3208.

Wang, H., & Dey, S. K. (2006). Roadmap to embryo implantation: clues from mouse models. *Nature Reviews Genetics*, *7*(3), 185-199.

Yang, Y., Zhu, Q. Y., & Liu, J. L. (2021). Deciphering mouse uterine receptivity for embryo implantation at single□cell resolution. *Cell proliferation*, *54*(11), e13128.

Yoshida, K., Line, J., Griffith, K., Wooldredge, A., & Cruz, Y. P. (2019). Progesterone signaling during pregnancy in the lab opossum, Monodelphis domestica. *Theriogenology, 136*, 101-110.

Zeller, & Freyer. (2001). Early ontogeny and placentation of the grey short□tailed opossum, Monodelphis domestica (Didelphidae: Marsupialia): Contribution to the reconstruction of the marsupial morphotype. *Journal of Zoological Systematics and Evolutionary Research, 39*(3), 137-158.

Materials and Methods

Animals and sample collection

C. porcellus (Charles River) were maintained at the University of Vienna according to Institutional Animal Care protocols. The estrus cycle was monitored by examination of vaginal membrane opening following Wilson et al. (2021). Females were mated in estrus at 3-4 months of age, and video recording was used to detect copulation during the night. Two individuals were used for sampling the implantation stage, 6.5 dpc and one was used as control 6 days after oestrus (early diestrus).

M.musculus (C57BL/6J) were maintained at the University of Vienna according to Institutional Animal Care protocols in a separate facility. The estrus cycle was monitored by vaginal swabbing following Ajayi & Akhigbe (2020). Copulation was determined by the presence of a copulatory plug and considered as day 0.5 post-copulation. Two individuals were used for sampling the implantation stage at 4.5 dpc and two were used for sampling the diestrus stage.

M. domestica were raised in a breeding colony at Yale University according to ethical protocols approved by the Yale University Institutional Animal Care and Use Committee (#2020-11313). Two individuals were used for sampling each stage: the non-cycling non-pregnant endometrium (n=2), 7.5 dpc (n=2) and 13.5 dpc (n=2, previously reported in Stadtmauer, Basanta et al., 2024). Video recording was used to assess the precise time of copulation. If multiple copulations were observed, the first was always used to establish 0 dpc.

Single-Cell Dissociation

Whole uterine horns were dissected into phosphate-buffered saline (PBS). Portions of ~ 0.2g per individual were minced into ~1 mm^3 cubes and transferred into a digestive solution containing 0.2 mg/mL Liberase TL (05401020001, Sigma) in 1800 µL PBS. The tissue was then incubated at 37ºC for 15 minutes and then passed 10 times through a 16-gauge needle attached to a 3-mL syringe. This process was repeated another two more times, the last time with a 18-gauge needle for complete dissociation. 2 mL of charcoal-stripped fetal bovine serum (100-199, Gemini) were added to stop digestion by inverting the tube several times. After that, the cell suspension was passed through a 70-µm cell strainer then a 40-µm cell strainer to get rid of any remaining chunks of tissue. The filtered cell suspension collected was centrifuged at 300 g for 5 minutes. The resulting pellet was resuspended in 1x ACK red blood cell lysis buffer (A1049201, Thermo-Fisher), incubated at room temperature for 5 minutes, and centrifuged again. The final pellet was resuspended in PBS containing 0.04% bovine serum albumen (A9647, Sigma) and Accumax (07921, Stem Cell Technologies). The resulting single cell suspension was assessed with a Cellometer (mouse, guinea

pig) or hemacytometer (opossum) to assess cell concentration and viability with trypan blue stain. Only cell suspensions with viability higher than 80-85% (rodent) or 70% (opossum) were used.

Library preparation and sequencing

Cells were captured using the 10X Chromium platform (3' chemistry, version 3). All libraries were generated according to manufacturer protocols (CG000315). Mouse and guinea pig libraries were generated at the University of Vienna and opossum libraries were generated at the Yale Center for Genomic Analysis.

Libraries were sequenced using an Illumina NovaSeq by the Yale Center for Genomic Analysis (*M. domestica*) at a read depth exceeding 20,000 reads/cell and at the Next Generation Sequencing Facility of the Vienna Biocenter (*C. porcellus* and *M. musculus*) at a read depth of around 400M reads per sample (Illumina NovaSeq S4 PE150 XP for *C. porcellus* and Illumina NovaSeq SP Assymetric 10X for *M. musculus*).

Single-Cell Data Analysis

Sequencing reads were aligned to reference genomes using the 10X Genomics CellRanger software (≥v7.0.0). *Monodelphis domestica*, *Cavia porcellus*, and *Mus musculus*, were mapped to their respective Ensembl genome annotations (ASM229v1 v104, cavPor3.0 v104, and GRCm39 v104, respectively).

Species-specific single-cell datasets were analyzed and annotated separately following seurat and scanpy standard functions and criteria to reveal species-specific cell types. Cells with fewer than 700 unique features or greater than 25% of transcripts of mitochondrial origin were filtered, as well as cells predicted to be doublets by doubletdetection (v4.2) (Gayoso & Shor, 2022). Library size normalization, log1p normalization, feature selection, dimensionality reduction, clustering and marker gene identification were performed using scanpy ≥ v1.9.1 (Wolf et al., 2018) for opossum and Seurat v4 (Hao et al., 2021) for mouse and guinea pig. Replicates belonging to the same species were corrected for batch effect using harmony (harmonypy, v0.0.9, r-harmony, v0.1) (Korsunsky et al., 2019), which adjusts principal components to aid in cluster delimitation but does not alter expression values. The optimal number of clusters was determined by comparison to those expressing unique gene expression confirmed by the use of cNMF v1.4.1 (Kotliar et al., 2019) gene expression module analysis. The optimal numbers of factors (K) were chosen based upon manual examination of stability-error curves as in Brückner et al. (2022).

Differential gene expression between pseudo-bulk transcriptomes of cell types from the same species at different time points was conducted using the DESeq2 method (v3.19, Love et al., 2014) and its python reimplementation pydeseq2 (v0.4.10, Muzellec et al., 2023). As luminal (LE) and glandular (GE) epithelial cluster cell abundances differed substantially across replicates, we merged all epithelial cell types into a single cluster ("eEpi") for the purposes of differential gene expression analysis. To identify differentially expressed ligands and receptors, the list of genes subjected to differential expression testing was subset to only genes encoding ligands, receptors, or the subunits of either in our ligand-receptor ground truth database used for communication inference. Gene set enrichment on differentially expressed genes was conducted using gseapy (v1.1.3; Fang et al., 2023) against the gene sets of single-molecule perturbations on cultured cell lines available in the NCBI gene expression omnibus (Enrichr "Gene_Pertubations_from_GEO_up").

Time-matched pre-implantation blastocyst scRNA-seq data were obtained from public repositories. These included opossum E7.5 bilaminar blastocyst (EMBL ArrayExpress E-MTAB-7515) (Mahadevaiah et al., 2020), mouse E4.5 blastocysts (NCBI Gene Expression Omnibus

GSE63266) (Nakamura et al., 2015), guinea pig E5.5 blastocysts (China National Center for Bioinformation PRJCA028188) (Guan et al., 2024), and human day 7 blastocysts (EMBL ArrayExpress E-MTAB-3929) (Petropoulos et al., 2016). Blastocyst cell types were annotated to identify trophectoderm using the original authors' annotations in the case of opossum and human. For mouse and guinea pig, where the authors did not provide original cell annotations, trophectoderm was identified as a *CDX2* and *GATA3*-expressing cell population following dimensional reduction and leiden clustering. Single-cell RNA-seq data from the human endometrium at mid-secretory stage (Marečková et al., 2024) and first trimester of pregnancy (Arutyunyan et al., 2023) were obtained from reproductivecellatlas.org.

Homology Inference by SAMap

Datasets from all species were integrated into a shared UMAP manifold using SAMap (v.1.3.4) (Tarashansky et al., 2021). Pairwise mapping scores between putative cell type clusters across species were calculated using the get_mapping_scores() function on the pooled transcriptome of all cells in each cluster. was used to calculate transcriptomic similarity scores between cells of different species.

Cell-Cell Communication Analysis

We inferred cell communication events between cell type transcriptomes using the method described in Stadtmauer, Basanta et al. (2024). Briefly, "human-equivalent transcriptomes" of each species were generated by mapping loci to their top BLAST hits using the BLAST+ graphs generated during the first stage of the SAMap pipeline. To maximize coverage, in cases of many:one human orthology, counts of all detected paralogs were pooled together. A ground truth ligand-receptor database was built as a manually extended fork of CellPhoneDB v5.0.0 (Garcia-Alonso et al., 2001) with additional curation and metadata. This modified list is archived at https://gitlab.com/dnjst/ViennaCPDB/. Cell interactions were inferred using expression thresholding with a cutoff of 0.2 (20% of cells in the cluster) for both ligand and receptor, or the least-expressed subunit if composed of multiple parts, using chinpy (v0.0.55; https://gitlab.com/dnjst/chinpy). Statistical testing for significantly cell type-enriched interactions were conducted using LIANA+ (v1.2.0) (Dimitrov et al., 2023).

For circos plots, depicted interactions are subset to those annotated as "Secreted Signaling" in our database, i.e. paracrine and endocrine peptide ligands, and "Small Molecule-Mediated", i.e. enzymes producing steroid hormones and other small molecules, but excluding extracellular matrix-mediated ligand-receptor interactions and those requiring direct cell-cell contact. For space reasons, the mouse and guinea pig interaction wheels were truncated to only the top 100 interactions as ordered by the LIANA+ "specificity_rank" metric. Differential expression analysis of ligands and receptors was subset only to Secreted Signaling peptides.

For Figure 9c, Pearson correlations were calculated between all mid-gestation cell type secreted signal repertoires (Stadtmauer, Basanta et al., 2024) and the peri-implantation uterine epithelium signaling repertoires (this study) using the corr() function of the pandas (v2.2.2) package. As with differential gene expression, uterine epithelial cell secretomes were generated from pooled populations of glandular and luminal sub-types ("eEpi"). Input data were boolean matrices of all ligands classified as Secreted Signaling (a total of 302), with a threshold proportion of cells in the cluster to be considered "on" of 0.10. Venn diagrams were plotted using the matplotlib_venn (v1.1.1) package and Jaccard indices of sets were calculated via the formula $J(A,B) = |A \cap B| / |A \cup B|$.

Differential Expression Analysis

To identify differentially expressed ligand and receptor signaling from epithelial to stromal cells at implantation, differential gene expression analysis was performed using pyDESeq2 (v0.4.10; Muzellec et al., 2023) on pseudo-bulk transcriptomes of peri-implantation and non-pregnant control stages grouped by cell type and stage (decoupleR-py v1.8.0; Badia-i-Mompel et al., 2022). Significantly changed genes were classified as those with a Benjamini-Hochberg adjusted Wald test p-value of less than 0.05. Only ligands with log2 fold-change values of mean ligand expression greater than 0.1 were included in Table S1.

Materials and methods citations

Ajayi, A. F., & Akhigbe, R. E. (2020). Staging of the estrous cycle and induction of estrus in experimental rodents: an update. *Fertility research and practice, 6*, 1-15.

Arutyunyan, A., Roberts, K., Troulé, K., Wong, F. C., Sheridan, M. A., Kats, I., Garcia-Alonso, L., Velten, B., Hool, R., Ruiz-Morales, E.R., Sancho-Serra, C., Shilts, J., Handfield, L., Marconato, L., Tuck, El., Gardner, L., Mazzeo, C.I., Li, Q., Kevala, I., Wright, G.J., Prigmore, E., Teichmann, S.A., Bayraktar, O.A., Moffet, A., Stegle, O., Turco, M.Y., & Vento-Tormo, R. (2023). Spatial multiomics map of trophoblast development in early pregnancy. *Nature*, *616*(7955), 143-151.

Badia-i-Mompel, P., Vélez Santiago, J., Braunger, J., Geiss, C., Dimitrov, D., Müller-Dott, S., Taus, P., Dugourd, A., Holland, C.H., Ramirez Flores, R.O., & Saez-Rodriguez, J. (2022). decoupleR: ensemble of computational methods to infer biological activities from omics data. *Bioinformatics Advances, 2*(1), vbac016.

Brückner, A., Badroos, J. M., Learsch, R. W., Yousefelahiyeh, M., Kitchen, S. A., & Parker, J. (2022). Evolutionary assembly of cooperating cell types in an animal chemical defense system. *Cell, 185*(7), 1257.

Dimitrov, D., Schäfer, P. S. L., Farr, E., Rodriguez Mier, P., Lobentanzer, S., Dugourd, A., Tanevski, J., Flores, R.O.R., & Saez-Rodriguez, J. (2023). LIANA+: an all-in-one cell-cell communication framework. *BioRxiv*, 2023-08. https://doi.org/10.1101/2023.08.19.553863.

Fang, Z., Liu, X., & Peltz, G. (2023). GSEApy: a comprehensive package for performing gene set enrichment analysis in Python. *Bioinformatics, 39*(1), btac757.

Garcia-Alonso, L., Handfield, L. F., Roberts, K., Nikolakopoulou, K., Fernando, R. C., Gardner, L., Woodhams, B., Arutyunyan, A., Polanski, K., Hoo, R., Sancho-Serra, C., Li, T., Kwakwa, K., Tuck, E., Kleshchevnikov V., Tarkowska, A., Porter, T., Mazzeo, C.I., van Dongen, S., Dabrowska, M., Vaskivskyi, V., Mahbubani, T., Park, J,., Jimenez-Linan, M., Campos, L., Kiselev, V., Lindskog, C., Ayuk, P., Prigmore, E., Stratton, M.R., Saeb-Parsy, K., Moffett, A., Moore, L., Bayraktar, O.A., Teichmann, S.A., Turco, M.Y., & Vento-Tormo, R. (2021). Mapping the temporal and spatial dynamics of the human endometrium in vivo and in vitro. *Nature genetics, 53*(12), 1698-1711.

Gayoso, A., & Shor, J. S. (2022). DoubletDetection: Doubletdetection v4. 2 (v4. 2). https://zenodo.org/records/6349517

Guan, T., Guo, J., Lin, R., Liu, J., Luo, R., Zhang, Z., Pei, D., & Liu, J. (2024). Single-cell analysis of preimplantation embryonic development in guinea pigs. *BMC genomics*, *25*(1), 911.

Hao, Y., Hao, S., Andersen-Nissen, E., Mauck, W. M., Zheng, S., Butler, A., Lee, M.J., Wilk, A.J., Darby, C., Zager, M., Hoffman, P., Stoeckius, M., Papelixi, E., Mimitou, E.P., Jain, J., Srivastava, A., Stuart, T., Fleming, L.M., Yeung, B., Rogers, A.J., McElrath, J.M., Blush, C.A., Gottardo, R., Smibert, P., & Satija, R. (2021). Integrated analysis of multimodal single-cell data. *Cell*, *184*(13), 3573-3587.

Korsunsky, I., Millard, N., Fan, J., Slowikowski, K., Zhang, F., Wei, K., Baglaenko, Y., Brenner, M., Loh, P., & Raychaudhuri, S. (2019). Fast, sensitive and accurate integration of single-cell data with Harmony. *Nature methods*, *16*(12), 1289-1296.

Kotliar, D., Veres, A., Nagy, M. A., Tabrizi, S., Hodis, E., Melton, D. A., & Sabeti, P. C. (2019). Identifying gene expression programs of cell-type identity and cellular activity with single-cell RNA-Seq. *Elife*, *8*, e43803.

Love, M. I., Huber, W., & Anders, S. (2014). Moderated estimation of fold change and dispersion for RNA-seq data with DESeq2. *Genome biology*, *15*, 550.

Mahadevaiah, S. K., Sangrithi, M. N., Hirota, T., & Turner, J. M. (2020). A single-cell transcriptome atlas of marsupial embryogenesis and X inactivation. *Nature*, *586*(7830), 612-617.

Marečková, M., Garcia-Alonso, L., Moullet, M., Lorenzi, V., Petryszak, R., Sancho-Serra, C., Oszlanczi, A., Mazzeo, C., I., Hoffmann, S., Krassowski, M., Garbutt, K., Kelaval., I, Gaitskell, K., & Vento-Tormo, R. (2024). An integrated single-cell reference atlas of the human endometrium. *Nature Genetics*, 1-13.

Muzellec, B., Teleńczuk, M., Cabeli, V., & Andreux, M. (2023). PyDESeq2: a python package for bulk RNA-seq differential expression analysis. *Bioinformatics*, *39*(9), btad547.

Nakamura, T., Yabuta, Y., Okamoto, I., Aramaki, S., Yokobayashi, S., Kurimoto, K., Sekiguchi, K., Nakagawa, M., Yamamoto, T., & Saitou, M. (2015). SC3-seq: a method for highly parallel and quantitative measurement of single-cell gene expression. *Nucleic acids research*, *43*(9), e60-e60.

Petropoulos, S., Edsgärd, D., Reinius, B., Deng, Q., Panula, S. P., Codeluppi, S., Plaza Reyes, A., Linnarsson, S., and Lanner, F. (2016). Single-cell RNA-seq reveals lineage and X chromosome dynamics in human preimplantation embryos. *Cell*, *165*(4), 1012-1026

Tarashansky, A. J., Musser, J. M., Khariton, M., Li, P., Arendt, D., Quake, S. R., & Wang, B. (2021). Mapping single-cell atlases throughout Metazoa unravels cell type evolution. *Elife*, *10*, *e*66747.

Wilson, R. L., Lampe, K., Matushewski, B. J., Regnault, T. R., & Jones, H. N. (2021). Time mating guinea pigs by monitoring changes to the vaginal membrane throughout the estrus cycle and with ultrasound confirmation. *Methods and Protocols*, *4*(3), 58.

Wolf, F. A., Angerer, P., & Theis, F. J. (2018). SCANPY: large-scale single-cell gene expression data analysis. *Genome biology*, *19*, 1-5.

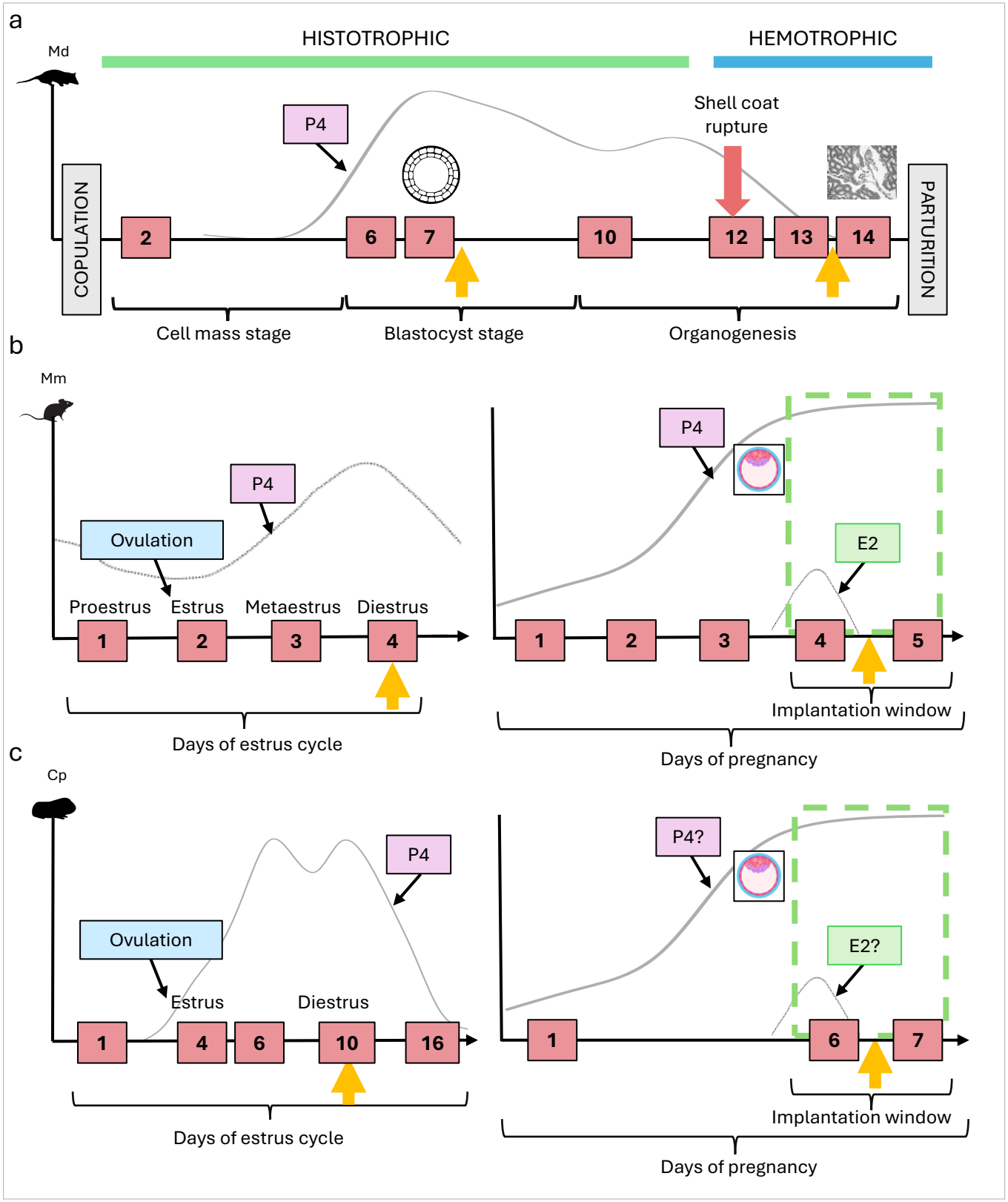

Figure 1. a) Diagram showing the gestation timeline of the opossum (adapted from Hansen (2017)). Yellow arrows indicate the days 7.5dpc and 13.5dpc included in our study. Progesterone peak at day 7 as reported by Hinds et al. (1992) **b)** Diagram showing mouse estrus cycle and window of implantation. Yellow arrows indicate the diestrus and implantation day (4.5dpc) used in the study. Progesterone patterns during first days of pregnancy as reported in Virgo & Bellward (1974) **c)** Diagram showing guinea pig estrus cycle and window of implantation. Yellow arrows indicate the diestrus (day 6 after ovulation) and implantation day (6.5 dpc) used in the study. Progesterone peak during the oestrus cycle as reported by Challis et al. (1971). Days of the estrus cycle in the guinea pig are approximate (proestrus lasts 2-4 days, the estrus 11h, metaestrus 4 days and diestrus from 8 to 19 days). P4 = progesterone, E2 = estrogen. Blastocyst icons and rest of hormonal patterns from BioRender. Mm= *Mus musculus*, Cp = *Cavia porcellus*, Md= *Monodelphis domestica*.

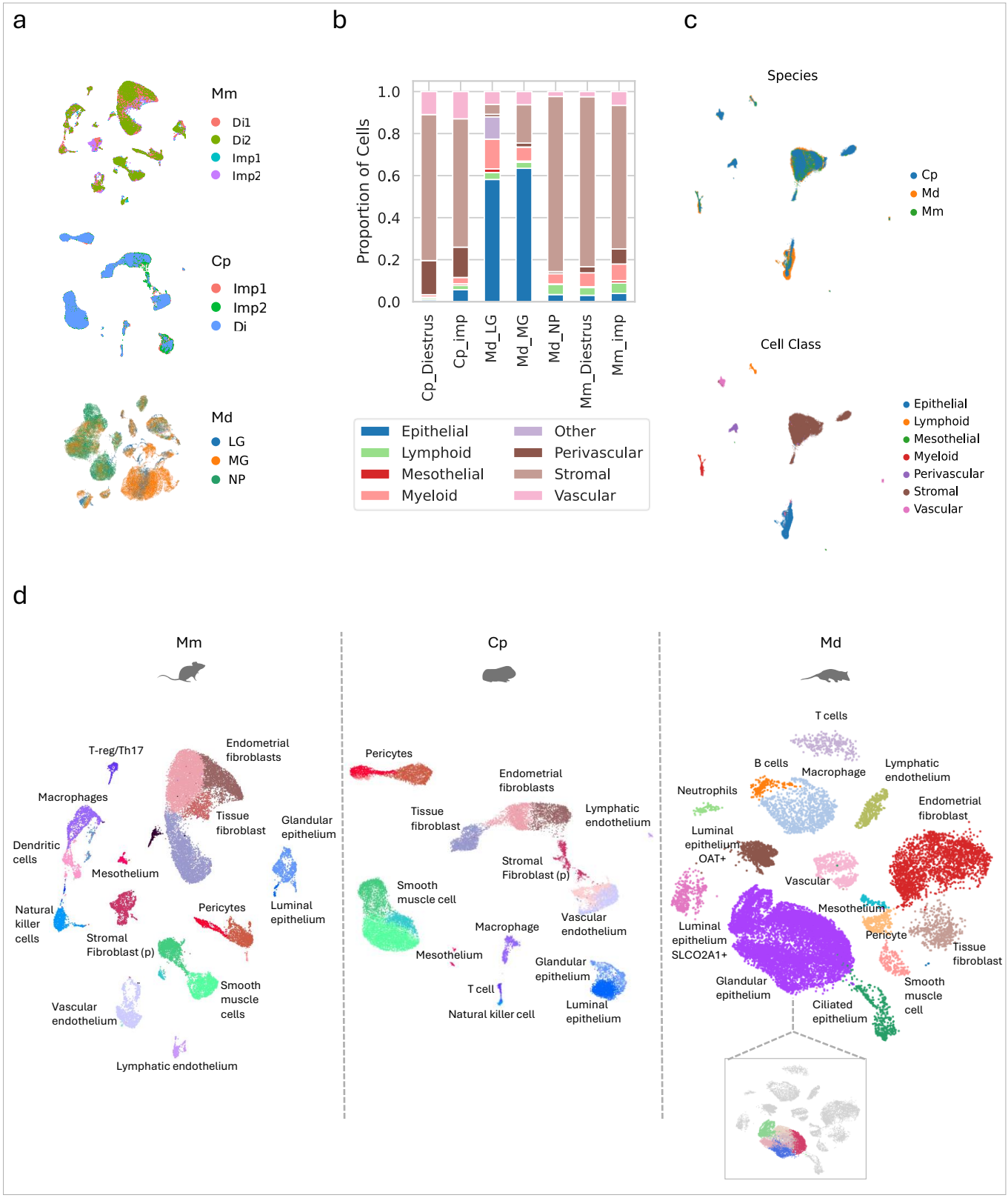

Figure 2. a) Harmony integration of samples (Imp= implantation, Di= diestrus, LG= late-gestation, MG= mid-gestation, NP= non-pregnant) within each species (Mm= *Mus musculus,* Cp= *Cavia porcellus*, Md= *Monodelphis domestica*) **b)** Relative cell class abundance per stage and in each species **c)** Major cell classes shared in the three species according to SAMap **d)** Individual UMAPs showing cell cluster identities resulting from the integration of pregnant and non-pregnant samples in mouse, guinea pig and opossum, along with the multiplicity of glandular clusters in the latter (for simplicity, placental cells present at late-gestation opossum are not shown). (p) = proliferating.

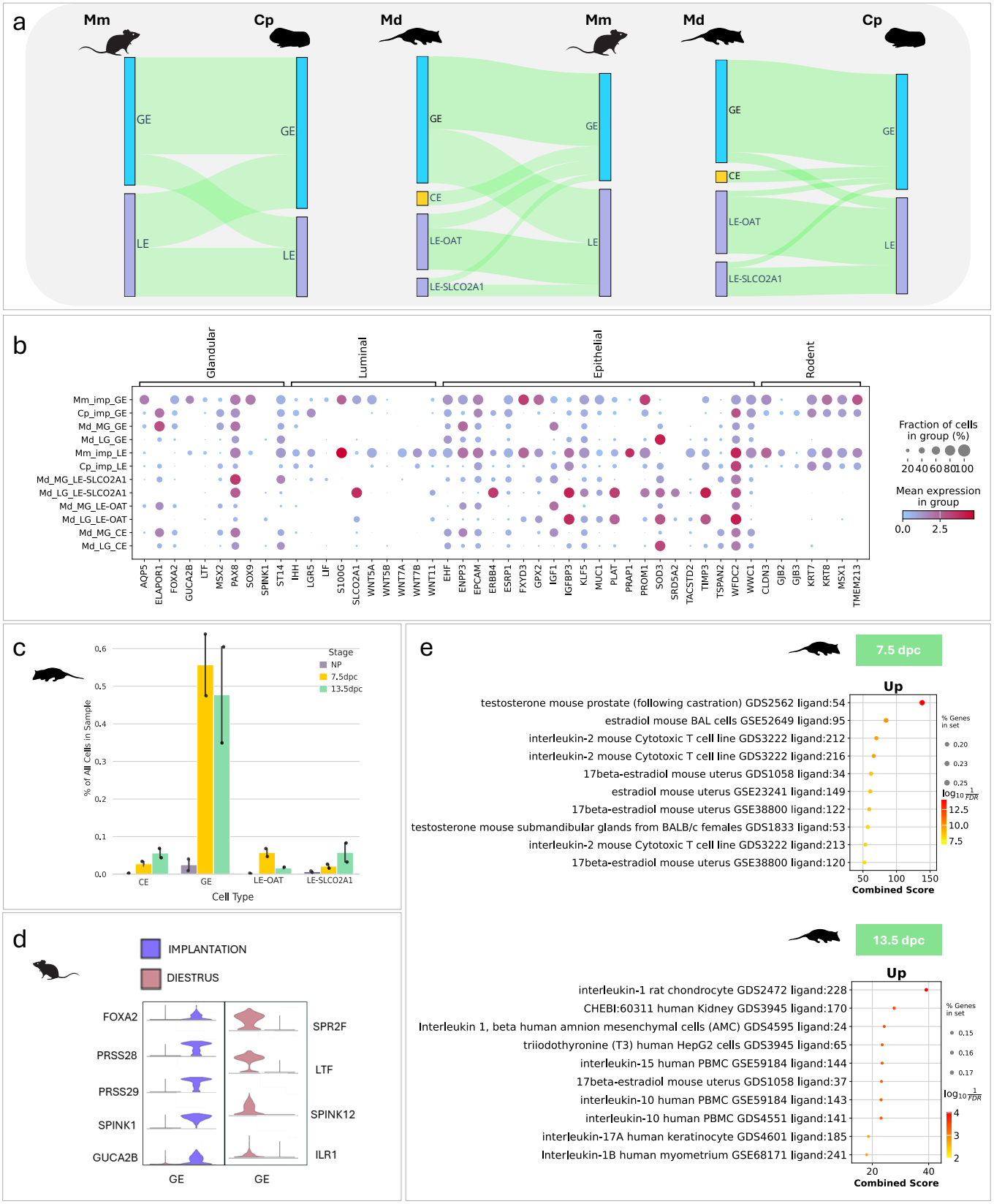

Figure 3. Epithelial cell type diversity, homology and gene expression dynamics. a) Sankey plots with bands proportial to SAMap transcriptomic similarity scores (0-1) of epithelial celll types across species **b)** Selected mouse, guinea pig and oposum epithelial maker genes at implantation (imp), oposum mid-gestation (MG) and late-gestation (LG). GE= glandular epithelium, LE= luminal epithelium, CE= ciliated epithelium. **c)** Abundance of the different epitelial cell types in the oposum across stages **d)** Differential expressed genes in mouse epithelial gland expression between implantation and diestrus **e)** Gene enrichment analysis on differentially expressed genes in the opossum glands between non-pregnant and 7.5 dpc and non-pregnant and 13.5 dpc using the database from EnrichR "Gene Perturbations from GEO up" gene set.

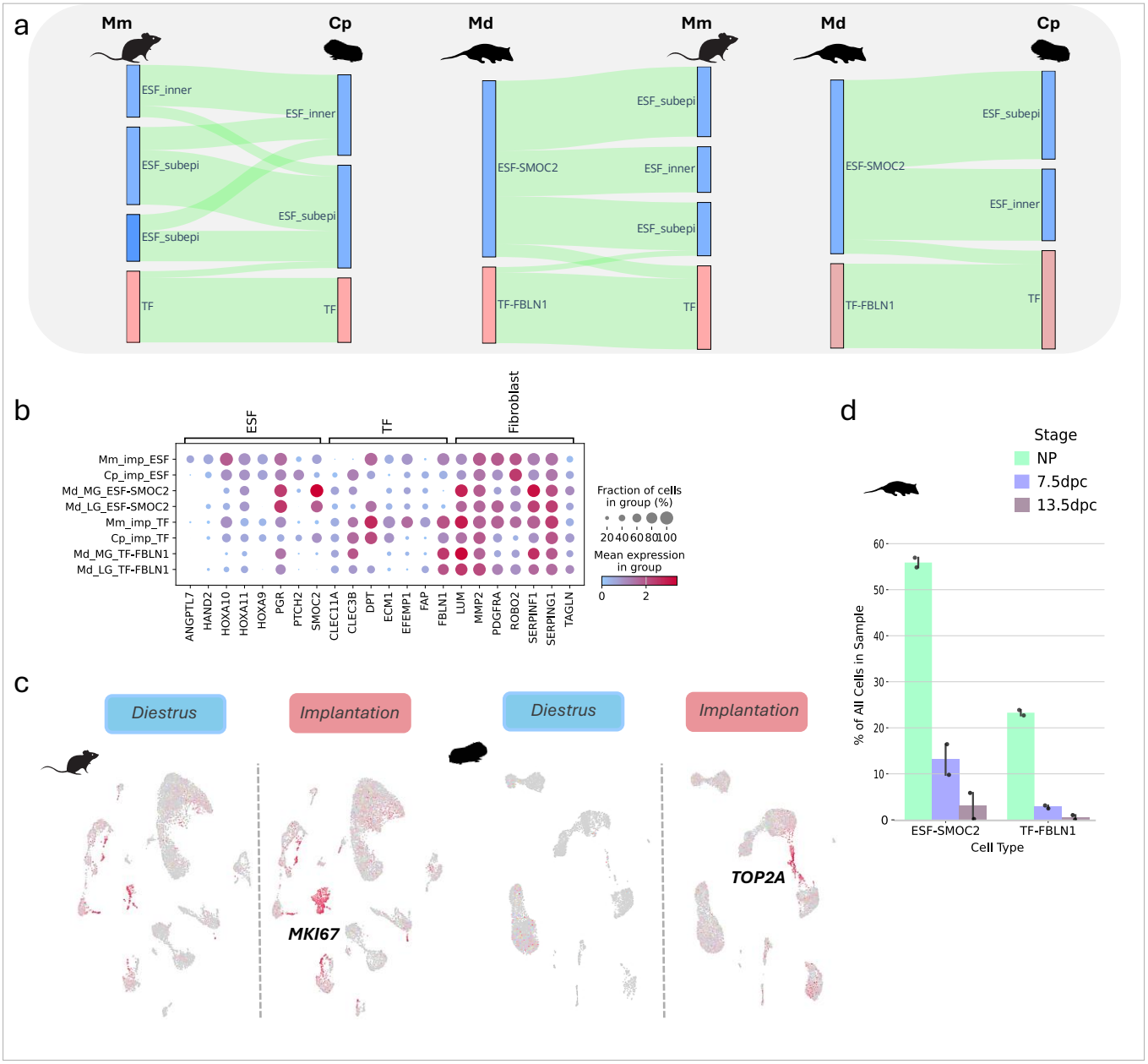

Figure 4. Fibroblast diversity, homology and abundance dynamics. a) Sankey plots showing SAMap transcriptomic similarity of the stromal cells across species. Thickness of the bands correspond to SAMap similarity scores (0-1) **b)** Expression of mice, guinea pig ad opossum fibroblast marker genes at same stages as in Figure 3b. ESF= endometrial stromal fibroblast, TF = tissue fibroblast **c)** Feature plots in rodents showing the proliferation of ESFs in implantation compared to diestrus through the expression of *MKI67* and *TOP2A* **d)** Barplot showing the abrupt decrease in stromal abundance towards late-gestation in the opossum. NP= non-pregnant.

	Mm 4.5 dpc	Cp 6.5 dpc	Md 7.5 dpc	Md 13.5 dpc
IHH- PTCH1	✓↑	✓↑	✓↑	X
LIF-LIFR	✓↑	X	✓↓	X
WNT-FZD	✓	✓	✓↓	X

Figure 5. Summary of upregulated and downregulated interactions from the epithelium to the endometrial stromal fibroblast compared to diestrus stages (in rodents) and the opossum non-pregnant/non-cycling endometrium. Detailed information in Table S4.

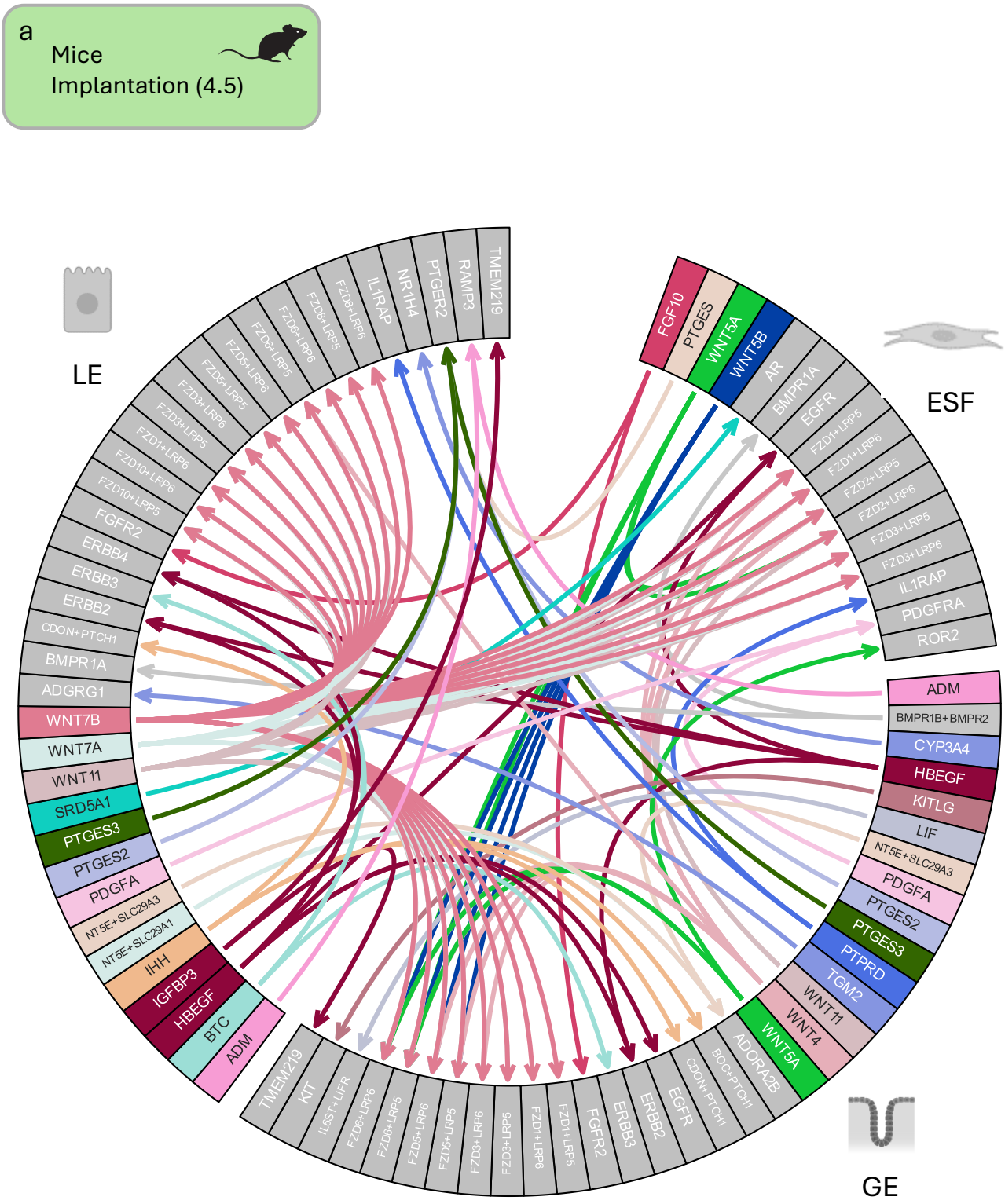

Figure 6. Mouse epithelial-stromal crosstalk. a) Circos lianaplots showing the first 125 putative (secreted-only) interactions sorted according to specificity rank involving the epithelial- stromal crosstalk at mouse peri-implantation. Ligands are shown in color and receptors in grey. Cell type icons from BioRender. LE = luminal epithelium. ESF = endometrial stromal fibroblast, GE = glandular epithelium.

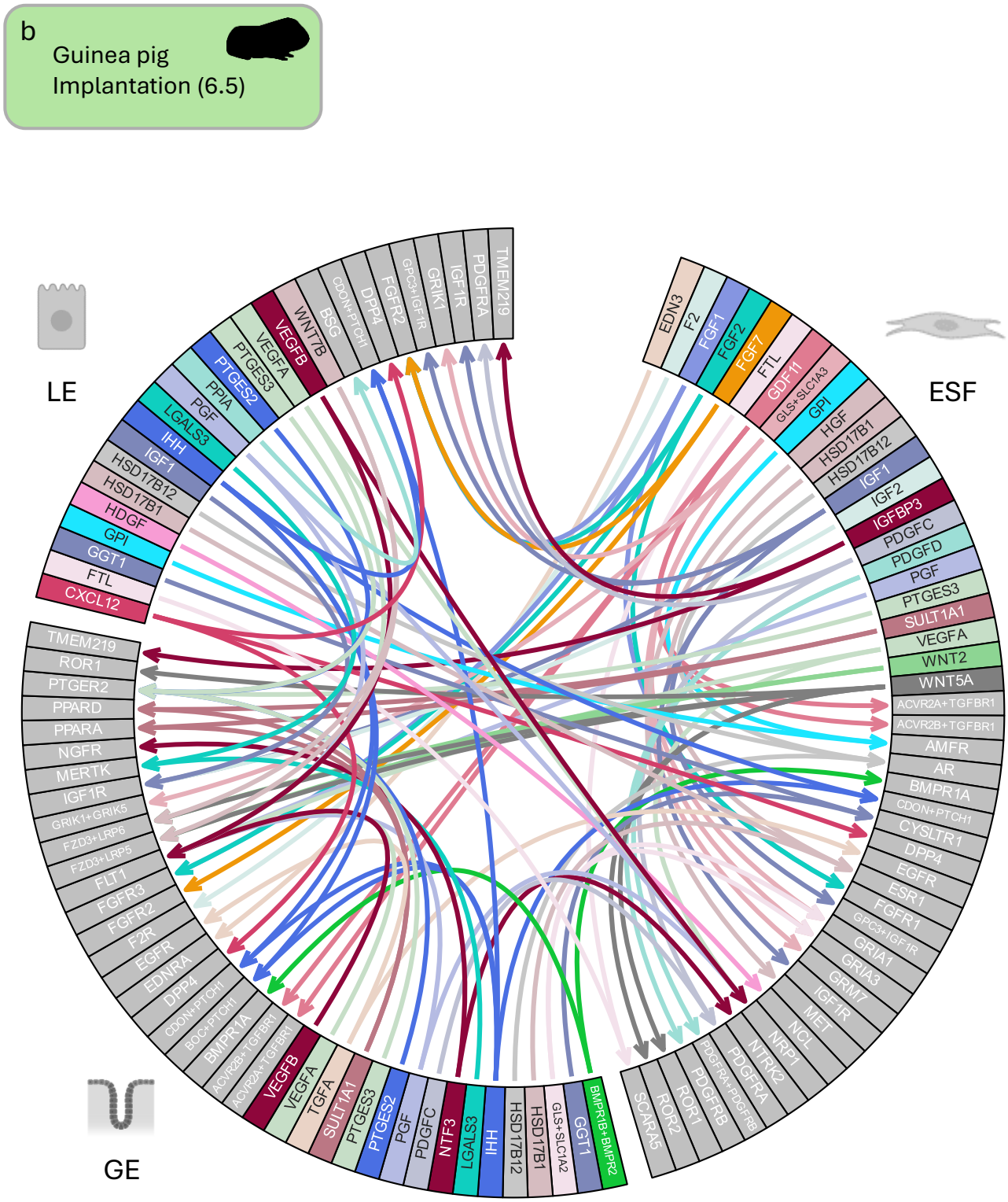

Figure 6. Guinea pig epithelial-stromal crosstalk. b) Circos lianaplots showing the first 125 putative (secreted-only) interactions sorted according to specificity rank involving the epithelial- stromal crosstalk at guinea pig peri-implantation. Ligands are shown in color and receptors in grey. Cell type icons from BioRender. LE = luminal epithelium. ESF = endometrial stromal fibroblast, GE = glandular epithelium.

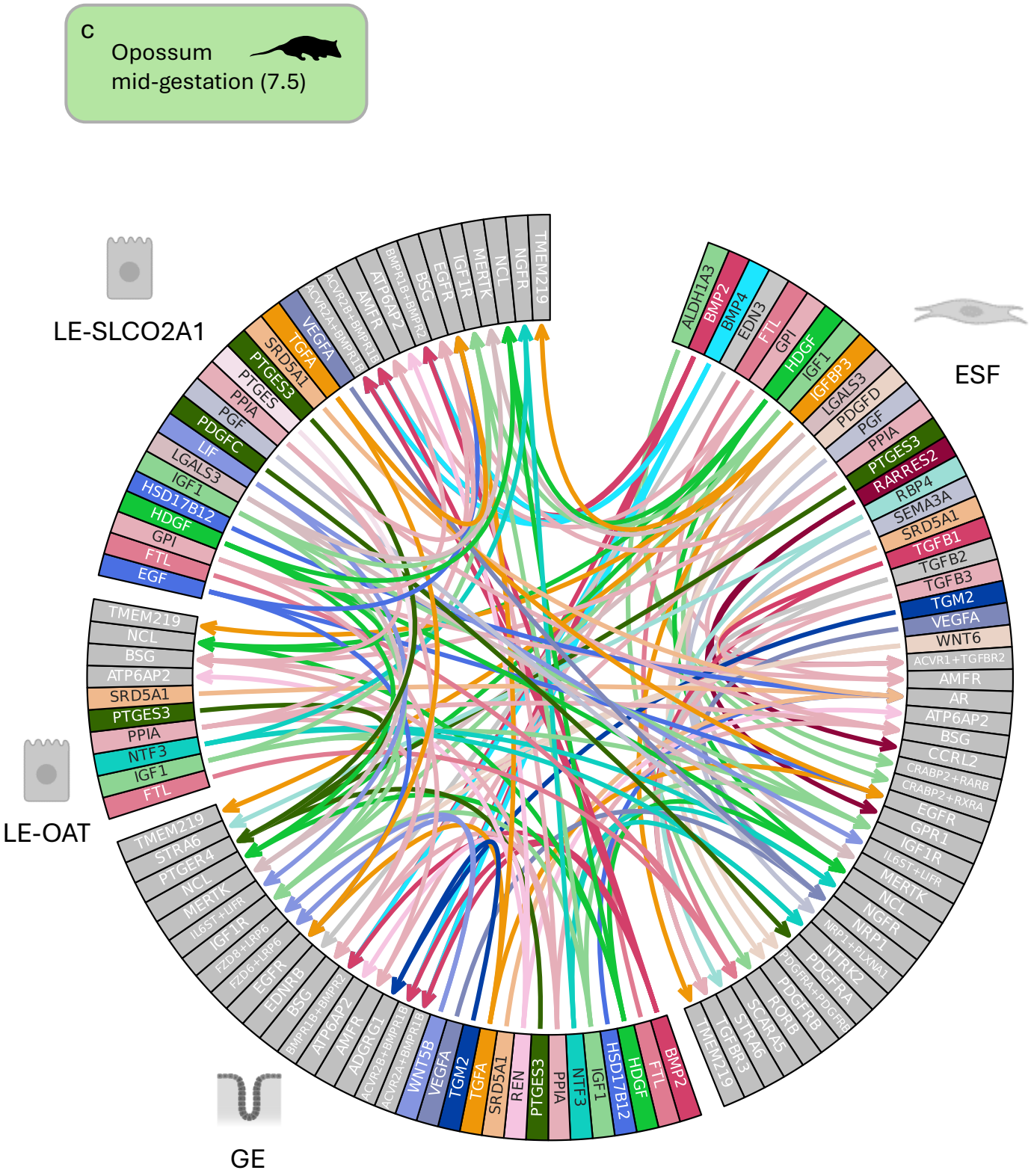

Figure 6. Mid-gestation opossum epithelial-stromal crosstalk. c) All the interactions (secreted-only) above threshold present at mid-gestation opossum (81). Ligands are shown in color and receptors in grey. Cell type icons from BioRender. Ligands are shown in color and receptors in grey. Cell type icons from BioRender. LE = luminal epithelium. ESF = endometrial stromal fibroblast, GE = glandular epithelium.

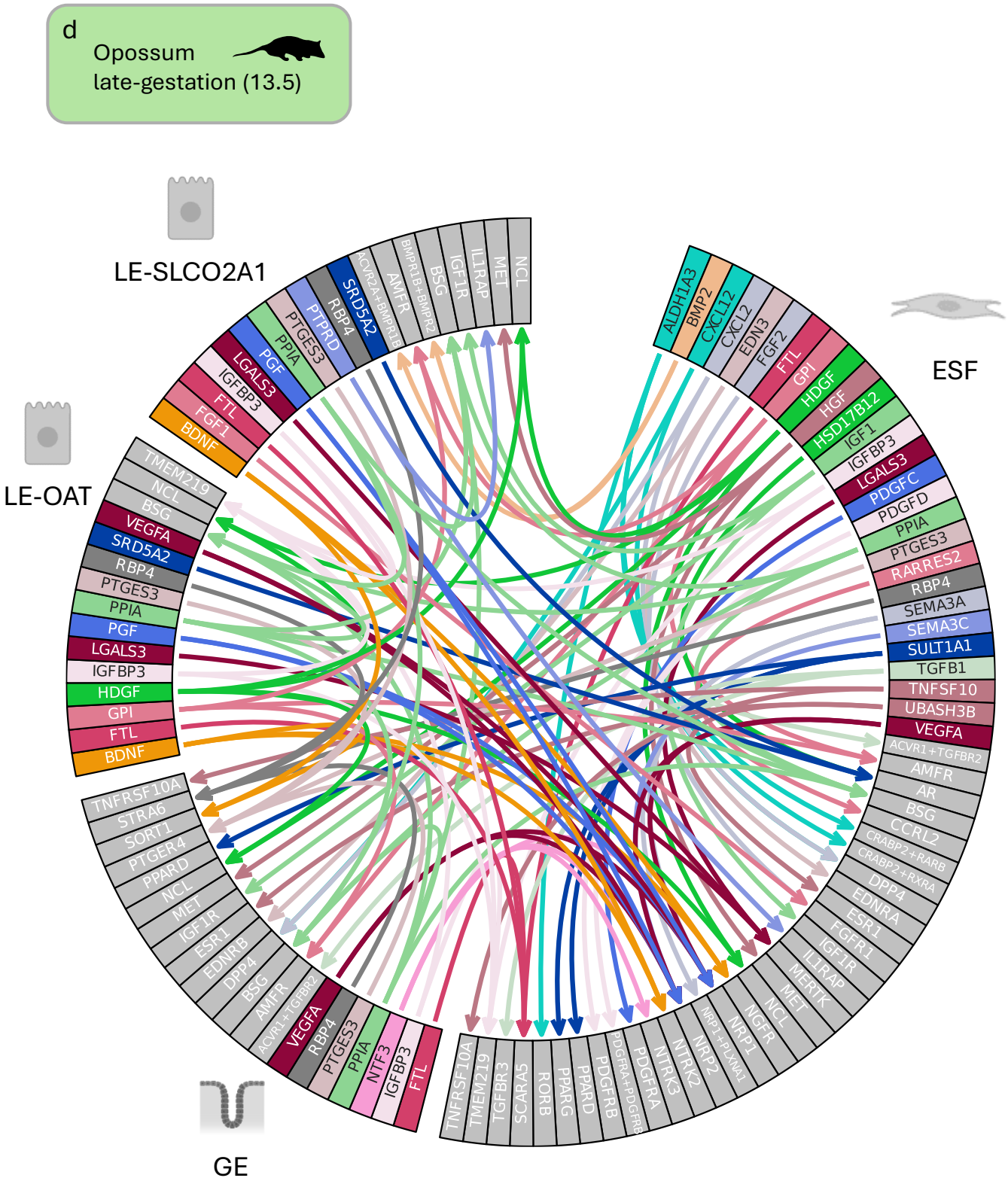

Figure 6. Late-gestation opossum epithelial-stromal crosstalk. d) All the interactions (secreted-only) above threshold present at late-gestation opossum (121). Ligands are shown in color and receptors in grey. Cell type icons from BioRender. Ligands are shown in color and receptors in grey. Cell type icons from BioRender. LE = luminal epithelium. ESF = endometrial stromal fibroblast, GE = glandular epithelium.

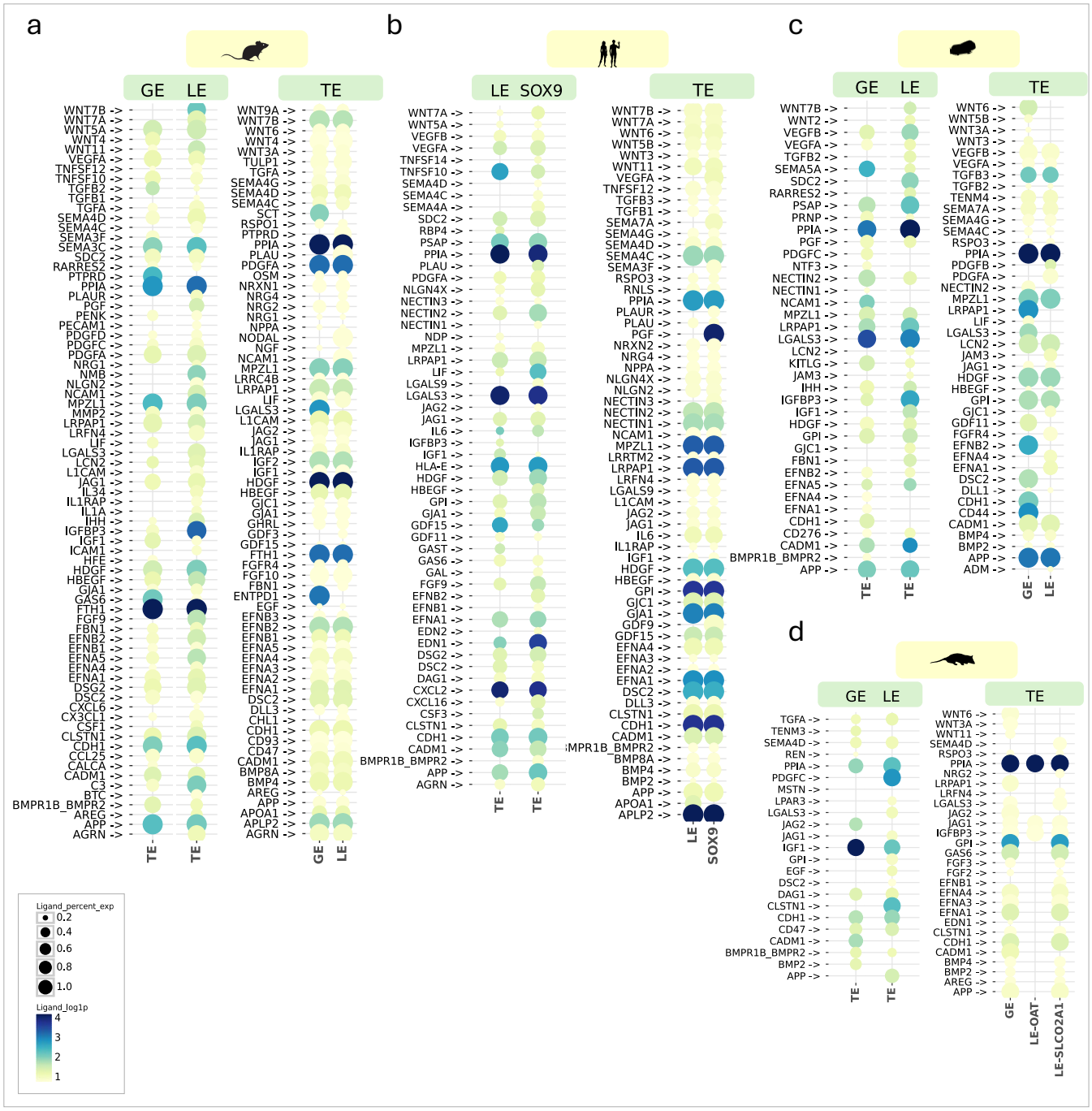

Figure 7. Dotplots showing inferred ligands from epithelial cells to the trophoectoderm (left) and from the trophoectoderm to epitelial cells (right) between in **a)** mouse **b)** human **c)** guinea pig and **d)** opossum. Interactions include cell-cell contact and ECM. All interactions showed passed the 20% expression threshold. TE = trophoectoderm, SOX9= human epithelial subtype as identified in (Marečková et al., 2024), LE= luminal epithelium, GE = glandular epithelium.

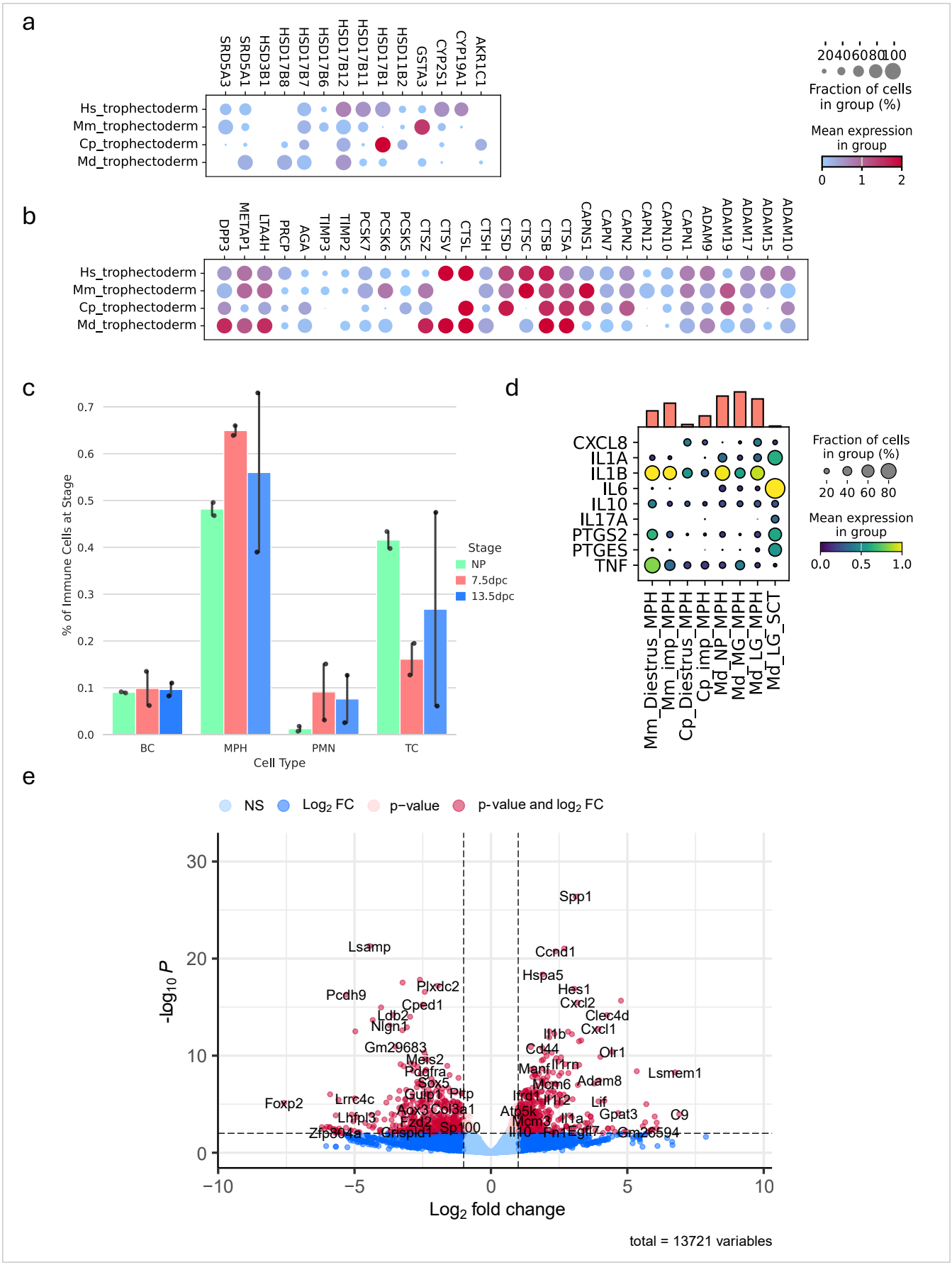

Figure 8. Blastocyst expression of **a)** small mediators involved in steroidogenesis and **b)** proteases in the human, mouse, guinea pig and oposum trophoectoderm **c)** Abundance of different immune cell types across stages in the opossum **d)** Expression of inflammatory mediators in macrophages (MPH) in different stages across species and in opossum syncytium (SCT). **e)** Volcano plot showing differential expression in mouse macrophages in implantation compared to diestrus.

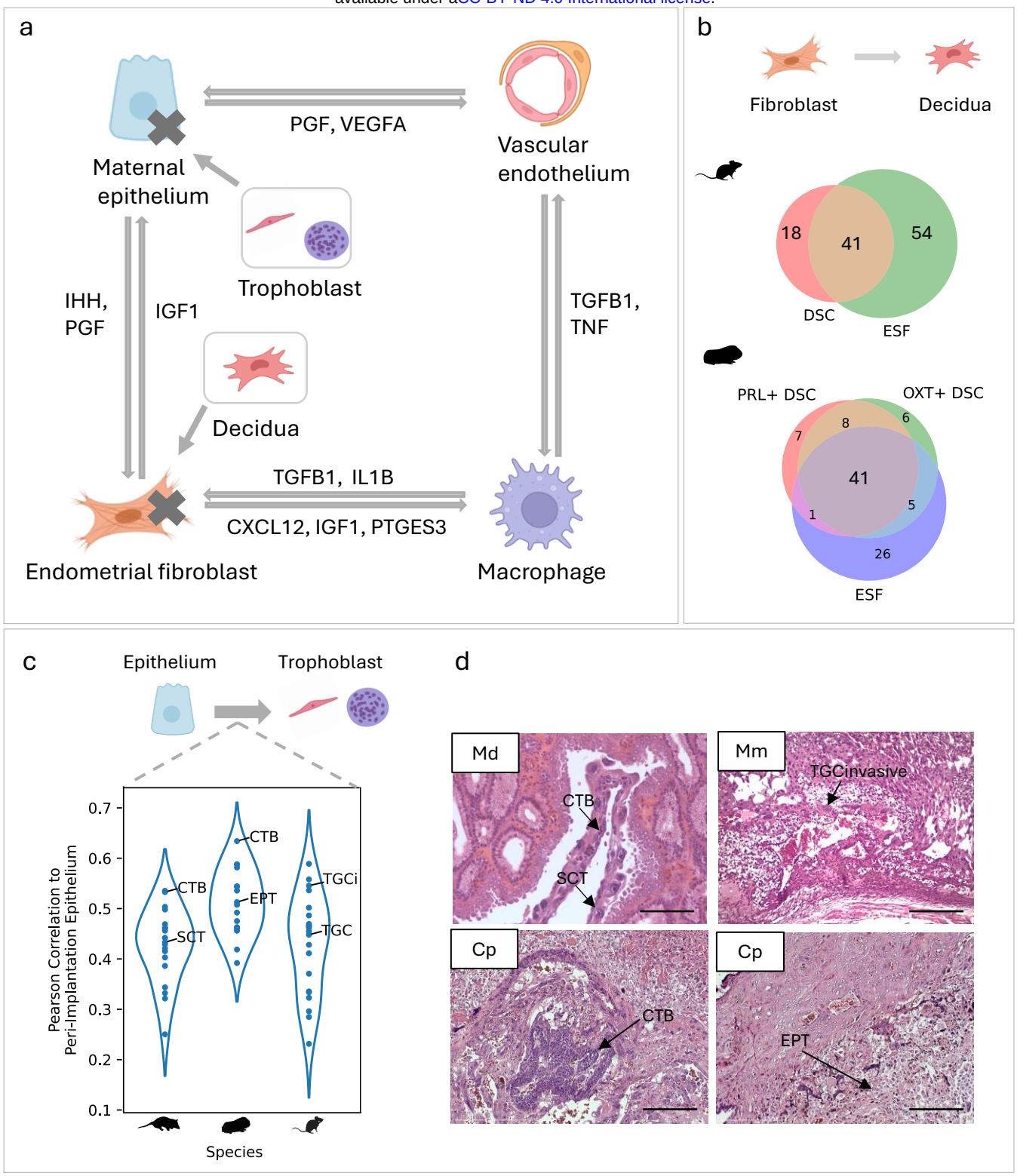

Figure 9. Signaling continuity between implantation and placentation. a) Conserved signaling interactions between the luminal epithelium, endothelium, macrophage and fibroblast in rodents and opossum, also showing the replacement of epithelial and fibroblast maternal cell types by the trophoblast and decidua during the transition to invasive placentation **b)** Venn diagram showing ligand expression overlap between ESF to decidua from implantation to mid-gestation in rodents **c)** Pearson correlation between the ligands expressed by the maternal epithelium and trophoblast populations of the same species, including the opossum **d)** Hematoxylin & Eosin showing the location of the same trophoblast populations across species. All scale bars correspond to 200 µm. DSD = decidual cell CTB = cytotrophoblast, SCT= syncytiotrophoblast, EPT = extraplacental trophoblast, TGCi = invasive giant trophoblast, TGC= giant trophoblast. Cell type icons from BioRender.

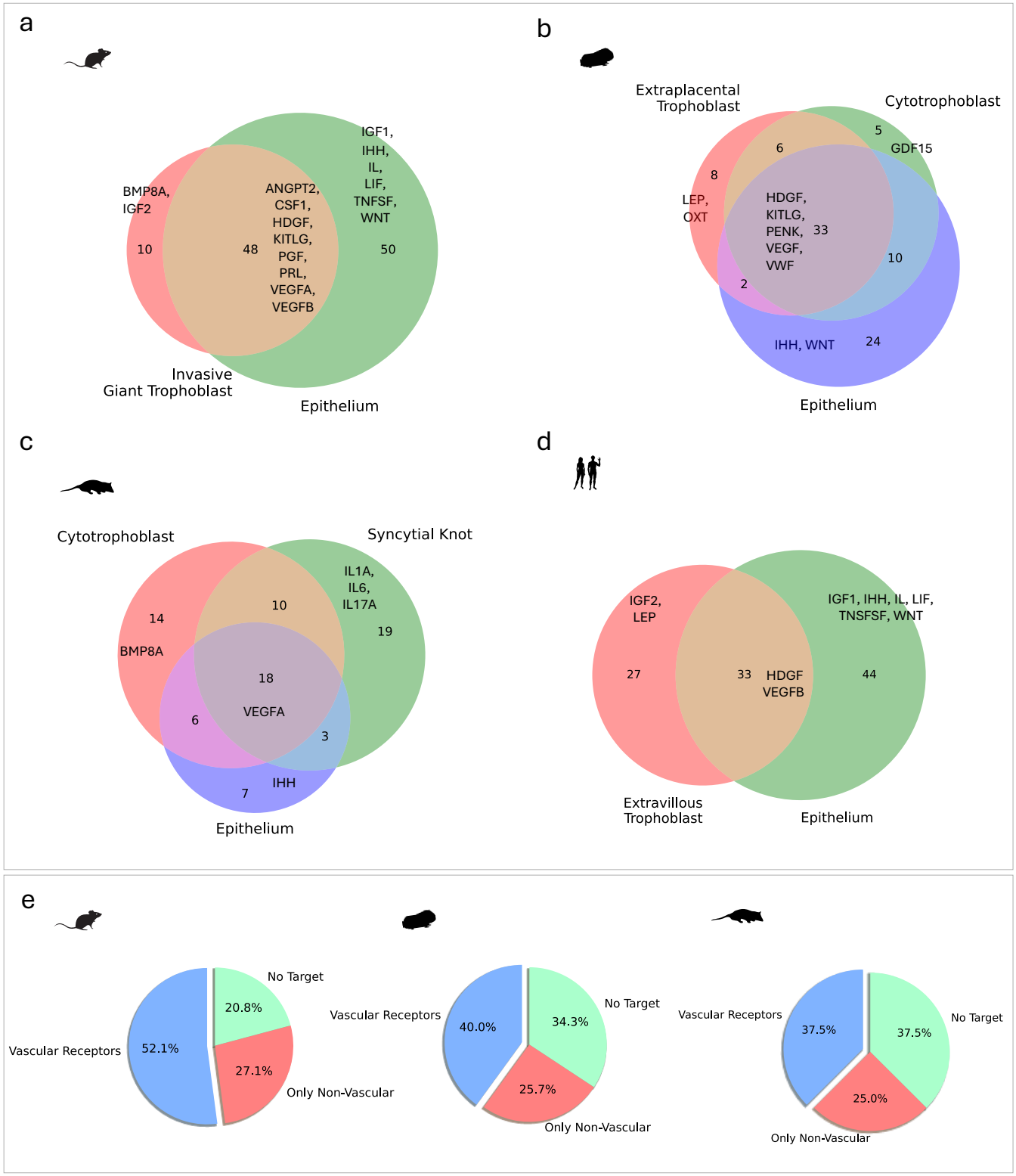

Figure 10. a) Venn diagram of the maternal epithelium of mouse peri-implantation and invasive trophoblast **b)** Venn diagram of the maternal epithelium of guinea pig peri-implantation and invasive trophoblast **c)** Venn diagram of the opossum day 7.5 epithelium and placental types at 13.5 dpc **d)** Venn diagram of the maternal epithelium and the human extravillous trophoblast **e)** Pie Charts showing the percentage of ligands with vascular receptors in mouse, guinea pig and opossum.

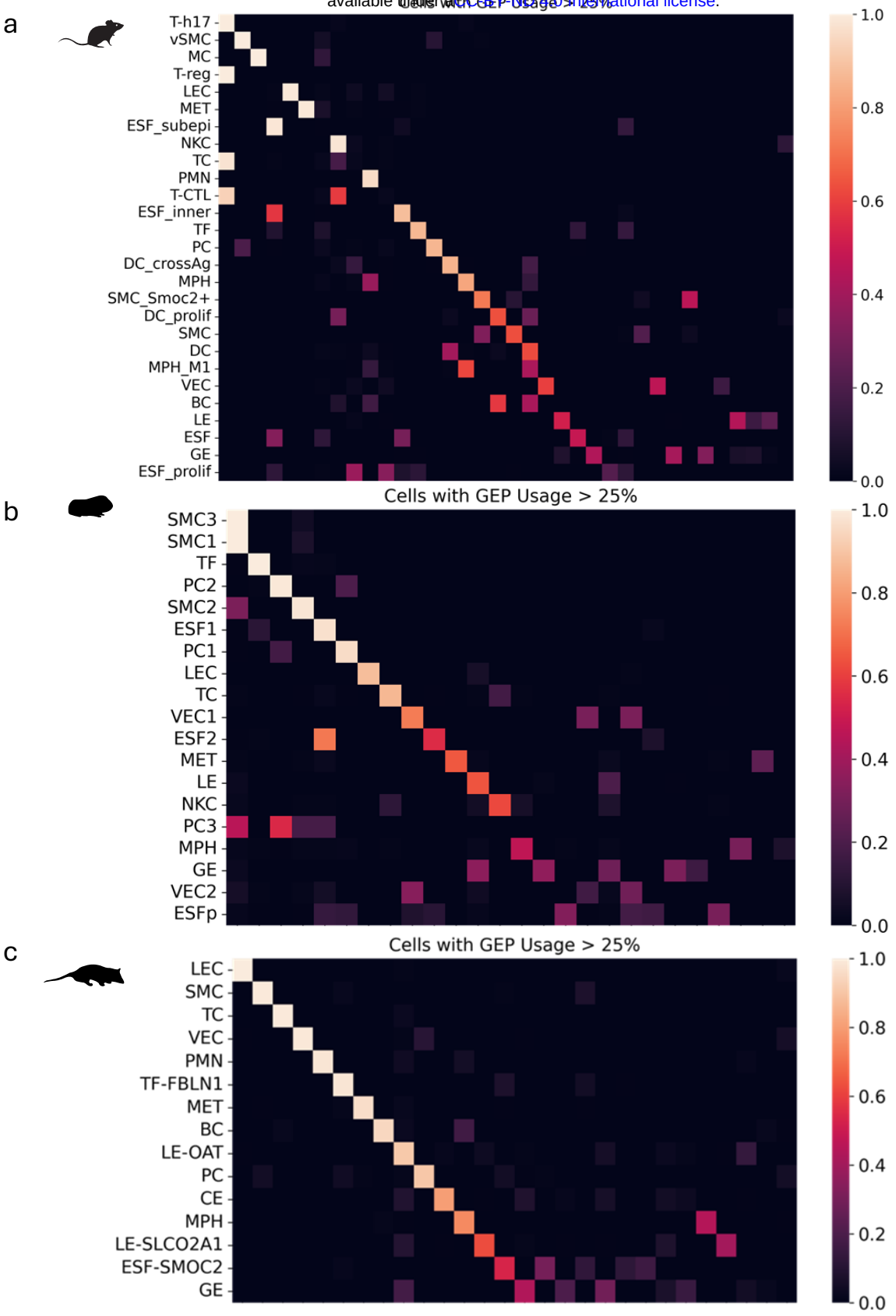

Figure S1. cNMF heatmaps showing percentage usage of gene expression programs (rows) in each maternal cell type in **(a)** mouse **(b)** guinea pig **(c)** and the opossum after harmony integration of stages within species.

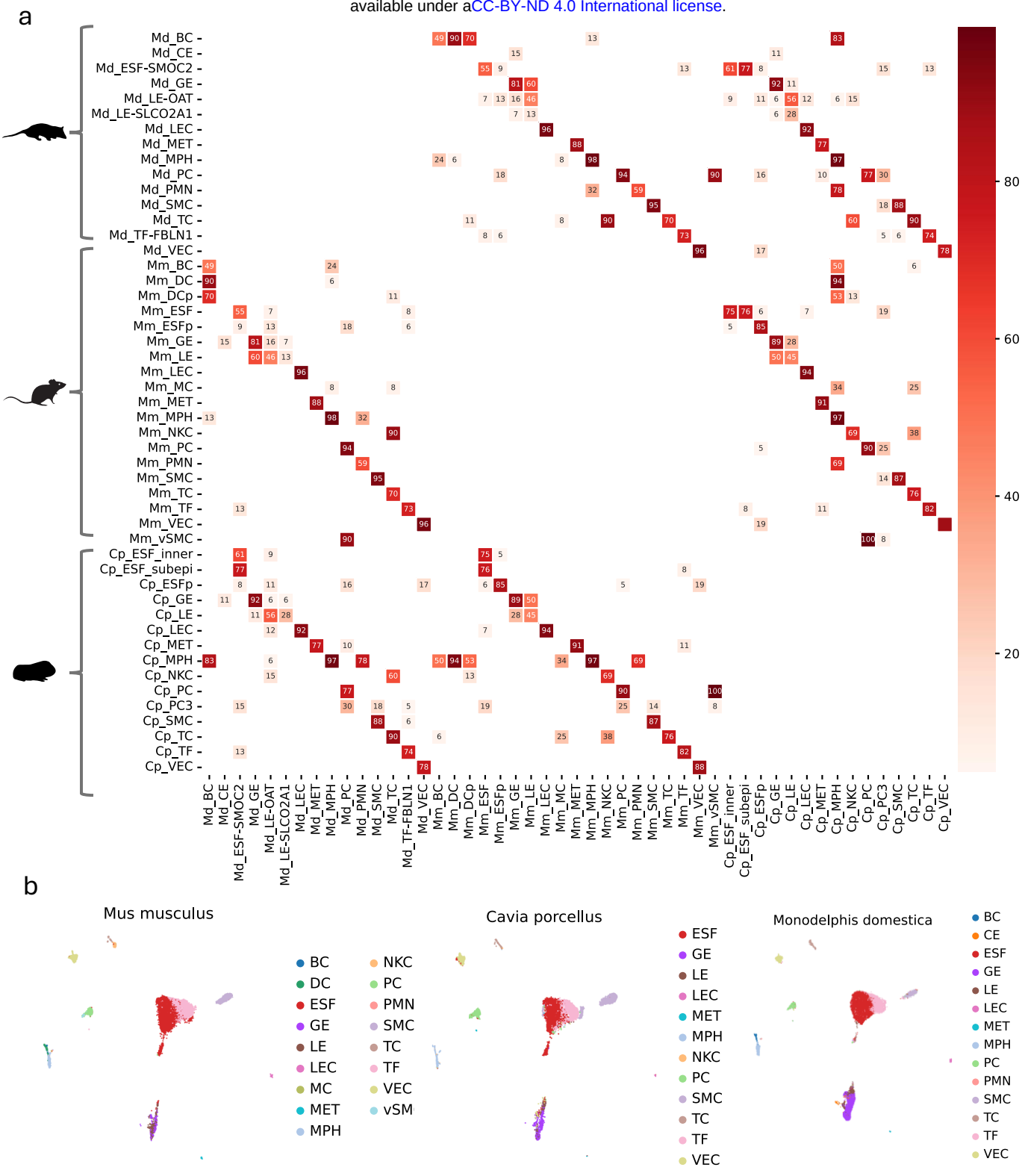

Figure S2. **a)** SAMap heatmap showing transcriptomic similarity scores across species **b)** Shared UMAP manifold across species, colored by the cell type as identified in the original, species-specific annotation, and showing correspondence across species. BC= B cell, DC= dendritic cell, ESF= endometrial stromal fibroblast, GE= glandular epithelium, LE = luminal epithelium, LEC = lymphatic endothelium, MC= mast cell, MET= mesothelial cell, MPH= macrophage, NKC= natural killer cell, PC= pericyte, PMN = polymorphonueclar neutrophils, SMC= smooth muscle cell, TC= T cell, TF = tissue fibroblast, VEC= vascular endothelium, vSM= vascular smooth muscle, CE= ciliated cell.

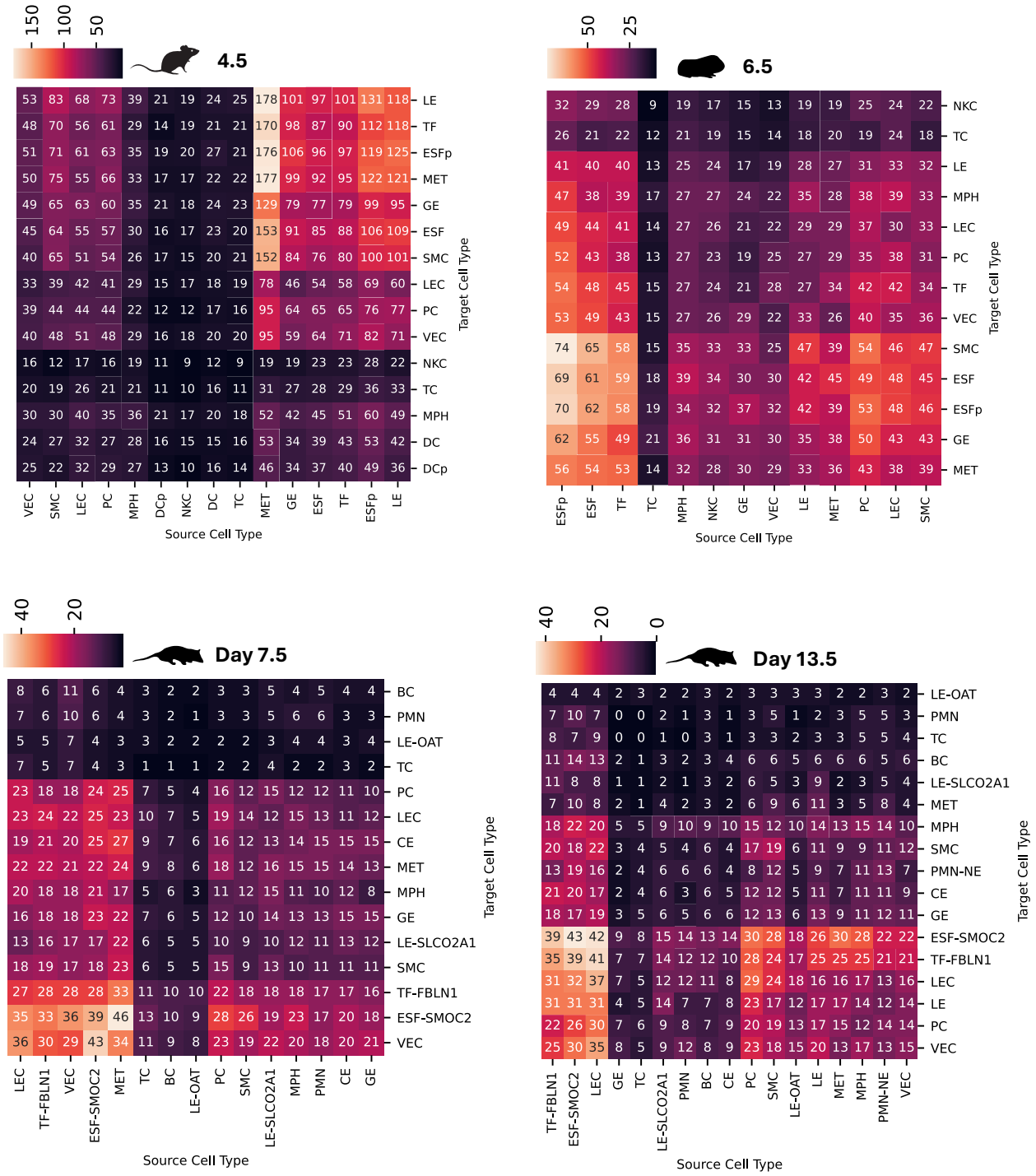

Figure S3. Heatmaps showing the numer of predicted secreted interactions above the 20% threshold between all clusters in mouse and guinea pig implantation (day 4.5 and 6.5 respectively), as well as in mid (day 7.5) and late-gestation opossum (day 13.5).